Technical Letter Report

[TLR-RES/DE/REB-2023-01]

Use of High Entropy Alloys (HEAs) in Future Nuclear Applications

Date:

January XX, 2023

Prepared as part of NRC's Future-Focused Research Program, by:

Adrien Couet and Nathan Curtis
University of Wisconsin-Madison

NRC Project Manager:

Wendy Reed
Senior Physical Scientist
Reactor Engineering Branch

Division of Engineering
Office of Nuclear Regulatory Research
U.S. Nuclear Regulatory Commission
Washington, DC 20555–0001

This report does not contain or imply legally binding requirements. Nor does this report establish or modify any regulatory guidance or positions of the U.S. Nuclear Regulatory Commission and is not binding on the Commission.

EXECUTIVE SUMMARY

High Entropy Alloys (HEAs) are a class of alloys which have been of interest since the mid-2000s for their potential for highly tailorable properties due to their departure from traditional alloy design by being composed of several principal elements rather than one or two. Such flexibility in their compositional space has led to several advancements in extreme environments, where conventional alloys are lacking in one or more properties for effective implementation. One such environment, nuclear reactors, is of particular interest due to the reported resistance to irradiation damage exhibited by HEAs. Although near-term commercial development of HEAs may not be likely, these recent studies have shown that HEAs could be developed with very desirable properties for advanced nuclear applications. As a means of analyzing currently published experimental results, a database of structural and electrochemical properties with accompanying Ashby plots has been constructed for comparison of HEAs and commercially available alloys, as well as a system to quickly identify alloys of interest. As a promising area of the HEA design space, variations of Cantor's alloy comprised of AlCuCrFeNi and AlCrFeMnNi prominently display improvements in desirable properties over many conventional alloys, including those currently utilized in light water reactors. With further exploration and refinement of the design space, HEAs could be an asset for advanced reactors and the nuclear industry as it continues to grow.

ACKNOWLEDGEMENTS

The authors of this report would like to thank the United States Nuclear Regulatory Commission for their financial support of this project (Award No. 31310021P0037).

TABLE OF CONTENTS

LIST OF FIGURES

1. INTRODUCTION

1.1 High Entropy Alloys

As opposed to most industrially relevant alloys used today (steels, aluminum alloys, titanium alloys, etc.), high-entropy alloys represent a fundamental departure from conventional metallurgy methodologies. Whereas conventional alloys are typically comprised of one or two principal elements with their properties tweaked by small alloying additions, HEAs consist of several principal elements often present in near equimolar quantities. The result is a material with a structure and properties that are not dictated primarily by a single element, but rather behave as an average of each primary constituent element. Beginning with two seminal papers in 2004, researchers Brian Cantor and Jien-Wei Yeh independently stumbled onto a trend in research which has subsequently grown exponentially [1].

In his paper, Cantor arc melted several alloys containing many elements in equiatomic ratios, including one 20-component ingot, with 5 at% each of Mn, Cr, Fe, Co, Ni, Cu, Ag, W, Mo, Nb, Al, Cd, Sn, Pb, Bi, Zn, Ge, Si, Sb, and Mg [2]. It was discovered that in the case of the equimolar 20-component alloy, far fewer phases formed than what was thermodynamically possible, per the Gibbs phase rule, and that within the ingot, a solid-solution phase of nearly equimolar Co-Cr-Fe-Mn-Ni had formed. Cantor then arc melted down a separate ingot of equimolar Co-Cr-Fe-Mn-Ni and found using X-ray diffraction (XRD) that the alloy exhibited a single, disordered FCC crystal structure – this alloy would go on to be referred to as the Cantor alloy or Cantor's alloy in literature [3], [4]. At the same time, Yeh et al. were examining CoCrCuFeNi, also found to be single-phase FCC, and the effects of Al additions on the transformation from FCC to BCC [5]. Motivating their alloy design was a pursuit of maximizing the configurational entropy in expanded alloy systems in the hope that this increase in entropy would be sufficient to suppress the formation of intermetallic compounds, which are often deleterious to the mechanical properties of materials. Yeh is credited with coining the term "high-entropy alloy", which he originally defined as equimolar alloys of five or more principal elements.

Note: Regarding nomenclature, as there appears to be no universally agreed upon standard, alloy compositions will hereinafter be written as their constituent elements in alphabetical order. For equimolar compositions, the alloys will simply be referred to as a string of their constituent elements symbols (e.g., CoCrFeMnNi), for non-equimolar compositions, subscripts will be added to denote the atomic percent of each constituent element (e.g., $Co_{10}Cr_{15}Fe_{35}Mn_{20}Ni_{20}$). Additionally, for the sake of completeness, Table 1 lists several terms that have been used to categorize the alloys compositionally in and around the realm of HEAs. Each of these terms uses different criteria to categorize alloys which can be restrictive depending on which source is defining it. Typically, the definitions use number of elements, ratio of elements, configurational entropy, total entropy, enthalpy of mixing, atomic radius mismatch, etc. to refer to a set of alloy systems, however as a result, many of the definitions overlap and some definitions are more exclusive than others. At their core, each definition seeks to envelope the region of composition space in the center of a phase diagram while eliminating the dilute solutions at the edges. Additionally, these definitions have evolved and, in some cases, relaxed over time. For example, while HEAs were initially defined as equiatomic alloys with five or more components, this was quickly broadened to five or more components ranging in concentration between 5-35 at% [5], which has since been expanded to include four elements and even some three element systems [6]. In some cases, it has been suggested that to be an HEA, the system must be a single-phase solid solution; however, since the entropy term in the Gibbs free energy is temperature dependent, this criterion is also arbitrarily temperature dependent since as temperatures approach absolute zero, the entropy contribution to the Gibbs free energy vanishes [7].

Table 1: *Alloy nomenclature from literature*.

Name	Reference
Baseless Alloys	[7]
Complex Concentrated Alloys (CCAs)	[8]
Compositionally Complex Alloys (CCAs)	[9]
Entropic Alloys	[10]
Equiatomic Multicomponent Alloys	[2]
High-Entropy Alloys (HEAs)	[5]
Medium-Entropy Alloys (MEAs)	[11]
Multicomponent Alloys	[2]
Multi-Principal Element Alloys (MPEAs)	[12]
Multinary Alloys	[13]
Single-Phase Concentrated Solid Solution Alloys (SP-CSAs)	[14]

To avoid becoming entangled in the ever-evolving nomenclature, an approach similar to that of Miracle and Senkov [15] has been taken within this text to include the greatest number of alloys that still capture the spirit of what it is to have a multi-principal component system whose properties are not dictated by any one primary element. Thus, as “high-entropy alloy” (HEA) is the term most often used to describe such systems, any alloy with no element present in greater concentration than 35 at% will be referred to hereinafter as an HEA. This should simplify the naming and still include concentrated ternary systems and systems that have elements present less than 5 at%, while still excluding binaries and many industrial alloys today that can be compositionally complex such as stainless steels and nickel-based super alloys. To describe alloys which have more than 35 at% of one element but still less than 50% of said element, the broader term “complex concentrated alloys” (CCAs) will be employed. While this unfortunately shares its acronym with compositionally complex alloys, there is no formal distinction between the two and thus they could be used interchangeably anyway. Though an alloy need not be a single-phase solid solution to be considered an HEA, much of the research in the area is focused on finding such alloys. There are reasons for this both from a standpoint of scientific understanding and of practicality. Thermodynamically speaking, under ambient conditions the most stable phase (or phases) of a system are dictated by the Gibbs free energy of mixing, given below, where ΔHmix is the enthalpy of mixing, T is temperature, and ΔSmix is the entropy of mixing:

$$\Delta Gmix = \Delta Hmix - T\Delta Smix \quad (1)$$

The most stable configuration is achieved when the Gibbs free energy is minimized. In most conventional alloys, the phases present are often dictated by heat of mixing, ΔHmix. If ΔHmix for the solid-solution phase is largely positive, the system will tend to phase separate as it is not energetically favorable for atoms of different species to mix with one another. If ΔHmix for any of the ordered phases is largely negative, the system will often form ordered compounds, such as intermetallic phases, so as to ensure atoms of different species are located next to one another. It is also possible that one phase is more energetically favorable than all others, but due to a non-negligible and positive ΔHmix the system can lower its energy by separating continuously into two regions sharing the same crystal structure but with disparate compositions, as is the case in a spinodal decomposition. These different microstructural outcomes are a reflection of how different

shapes and sizes of the Gibbs free energy curves can produce different combinations of thermodynamically stable phases. Due to the compositional complexity from several principal alloying elements, the system will typically exhibit a large entropy contribution to Gibbs free energy. This can surpass the enthalpy contribution in Gibbs free energy for ordered phases in relevant operating temperatures. The end result is an alloy which is thermodynamically favored to maintain a single-phased microstructure.

Due to the compositional complexity of HEAs which exist in a phase space distant from our dilute solution approximations, their properties can be difficult to predict. This difficulty in material property predictions can be exacerbated by the presence of multiple phases. As such, studying the mechanisms responsible for property tuning in single-phase HEAs may be more insightful by eliminating the effects of secondary phases. Consequently, several criteria have been used to predict single-phase solid-solution HEAs and often incorporate the relative magnitude of ΔSmix and ΔHmix, as well as other more traditional means of predicting solid solubility such as the Hume-Rothery rules.

1.2 Manufacturing of High Entropy Alloys

Early HEA production was dominated by modifications of conventional methods; induction melting is common and still used for larger bulk castings, particularly with variations of Cantor's alloy [2], [3]. There are concerns, however, with casting methods for HEAs attributable to the defects introduced during production. When conventional alloys are cast, they often require re-melting and/or additional heat treatment to remove chemical heterogeneities and release stresses within the casting. This is a significant hindrance to HEA performance since their atypical compositions can lead to even more severe chemical and phase segregation [1].

Another conventional production method favored in HEA production is vacuum arc melting. While this process is effective for melting and casting material, the low pressures and high temperatures present can result in the volatilization of elements, the most notable of which being manganese. Vacuum arc melting is even more problematic for refractory HEAs (RHEAs), where embrittlement from even minor oxygen, carbon, and nitrogen impurities can produce severe intergranular cracking [16], [17]. A method of manufacturing RHEAs to minimize this embrittlement is powder sintering. The problems encountered by each of these conventional methods have been addressed in part by both powder metallurgy and additive manufacturing.

Sintering is a powder-based method which uses pre-alloyed and mechanically mixed powders to achieve a fully dense material through high temperature and pressure. One method used frequently for HEAs is spark plasma sintering, which has been favored for RHEAs similarly to ceramics due to its ability to form near-full density materials quickly [18]. The combination of high temperatures and fast sintering times can limit grain size, chemical segregation, and residual stresses in the material. This does, however, require expensive metal powders and produces very simple and limited geometries. For powder-based production of more complex parts, the industry relies on additive manufacturing.

Many additive manufacturing methods employable fall under two categories, laser metal deposition (LMD) and selective melting via laser or electron beam. LMD utilizes a laser to melt the substrate from which the component will be built, and then a powder is blown onto the substrate, adhering to the locally melted area. This is continued in successive layers until the

component has been built upon the substrate, after which it is removed mechanically [19], [20]. Laser powder bed fusion (LPBF) produces parts by tracing a laser across the feed material (commonly a bed of powder) to produce a layer of material. This is followed by lowering of the part, refreshing the material available, and melting another layer of material on top of the current component repeatedly until the component is produced [19], [20]. The result is the capability to produce complex geometries, and LPBF's rapid cooling rate minimizes chemical segregation.

These methods are not without shortcomings, however: they are expensive due to their high material costs, and residual stresses from additive manufacturing still require heat treatment of parts in post-processing. Furthermore, the fast-cooling rates result in a metastable material which does not accurately reflect potential bulk material performance, especially in high temperature applications. The usage of laser or electron beam heating of the surface can lead to keyholing and gas entrapment defects in additive manufacturing, much like their welding counterparts [21]–[23]. Despite these concerns, additive manufacturing-produced HEA components yield promising results, displaying superior properties both mechanically and electrochemically [24]. In addition, the reduction of secondary phases and precipitates provides greater clarity when studying HEA properties, laying the groundwork for effective and impactful research.

2. IMPORTANCE OF HIGH ENTROPY ALLOYS IN THE NUCLEAR INDUSTRY

High-entropy alloys have demonstrated a broad range of promising properties for both structural materials and functional materials including markedly higher yield strengths than Ni-based superalloys at high temperatures [25], fracture toughness comparable to the best cryogenic steels at low temperatures [26], high-temperature oxidation resistance [27], and superplastic behavior [28], as well as efficient catalysis of H_2 and CO_2 [29] and the largest magnetocaloric effect experimentally observed in a material [30]. But by far, the most relevant and intriguing property of HEAs for nuclear application is their microstructural response to irradiation damage. Many experimental studies have shown that certain HEA compositions outperform their less compositionally complex counterparts under irradiation [14], [31]–[37], especially when comparing void swelling behavior. One such study evaluated the relative swelling amount of different equimolar HEAs and CCAs subjected to 3-MeV Ni ion irradiation to a fluence of $5x10^{16}$ ions/cm^2, corresponding to a peak damage of 53 dpa, at an irradiation temperature of 500 °C [34]. It found that with increasing compositional complexity (Ni→NiCo→NiCoCr→NiCoFeCrMn) the amount of void swelling decreases from ~7% down to nearly immeasurable. While the differences in void swelling behavior are striking, the mechanistic reason for these differences in behavior remains unclear.

To understand the origins of the apparent irradiation tolerance exhibited by HEAs, it is important to first understand the damage mechanisms that occur during irradiation, particularly those which contribute to the growth of voids within the material.

Irradiation damage begins with an incident source of excess energy which can come from waves, ions, or fission products. When the energy is great enough, it will knock an atom off its lattice site in the crystalline material, creating a pair of point defects, usually a vacancy and an interstitial, called a Frenkel pair [38]. While the displaced atoms can relax to their original positions athermally during irradiation induced cascade quenching, during the short timescale of energy dissipation, the interstitial atoms may not have the necessary energy to relax back to a vacant site, leaving a surviving vacant lattice site and introducing an interstitial atom into the matrix [39]. This description only considers a singular atom's displacement, when irradiated materials see this occurring all along the exposed surface. When considering this general bulk interaction with irradiation, the development of macroscopic radiation defects can be understood.

Beginning with the first atom subjected to the energy from irradiation, the primary knock-on atom (PKA), it is expected that it will also hit other atoms within the lattice as it is quickly scattered; the resulting cascade of defect production and partial recombination occurs on the order of picoseconds and will occur for several other local cascades at the same time [38]. The rapid cooling of the microstructure following the incident energy's dissipation will inhibit the full recombination of defects, leaving many Frenkel pairs within the matrix. Since it is more thermodynamically favorable for vacancies to position themselves next to other vacancies [39], open lattice sites will diffuse and combine at the elevated temperatures nuclear reactors operate at, leading to greater areas generally "filled" by vacancies. This is the basis for void formation during irradiation, and the consequent voids and redistribution of atoms interstitially elsewhere in the lattice increases the overall volume of the system. Both vacancies and interstitial defects are

contributors to dimensional changes in irradiated materials, but the formation of voids is usually referred as swelling [38], [39].

Many mechanisms have been proposed in literature that provide potential explanations for the observed radiation tolerance of HEAs, which will be described in chronological order over the evolution of irradiation damage in a material as follows:

More recombination during damage cascade. From the Kinchin-Pease (KP) model, the number of defects produced from a single PKA is only dependent on the ratio of the PKA energy to the displacement energy (the energy required to form a vacancy/self-interstitial atom (SIA) pair). As such, it follows that the number of defects produced from a PKA of a given energy should be the same in an HEA as in a pure metal if their displacement energies are comparable, which is already a charitable assumption since some simulations have shown HEAs have a lower displacement energy than pure metals [40]. If the number of defects initially created during the damage cascade in an HEA is equal to or greater than a pure metal, one possibility for the apparent irradiation tolerance of HEAs is that more recombination of these point defects occurs before the heat dissipates from the damage cascade and quenches in the surviving defects. Since the length scales and timescales of the damage cascade are prohibitively short for experimental observation, support for this proposed mechanism comes primarily from simulation. Specifically of interest is the increase in phonon scattering in HEAs and CCAs relative to pure or less compositionally complex metals. While electrons are the primary heat carriers in metals under most circumstances, during the damage cascade, energy is imparted directly to the atoms and heat transport is dictated primarily by phonons rather than electrons, based on the difference between the lattice and electronic heat capacities [41], [42]. Since populating a lattice with different elements leads to greater phonon scattering, based on the difference in masses and interatomic forces between the different atom species, HEAs and CCAs would be expected to have lower lattice thermal conductivity [43]. During the damage cascade, a lower lattice thermal conductivity would imply that the heat deposited during the damage cascade remains localized longer before being dissipated in the surrounding material, which would allow more time for recombination of point defects to occur before the surviving defects are quenched in. Indeed, differences in lattice thermal conductivity have been used to explain the decrease in void swelling with increasing material complexity seen in the swelling behavior of Ni, NiCo, and NiFe [44], [45]. However, simulations from other studies have shown similar and sometimes more surviving point defects following the damage cascade in HEAs compared to less complex alloys [40], [46], so it remains unclear if enhanced recombination exists in HEAs, and if so, to what extent it improves the overall irradiation resistance of the material.

Sluggish diffusion of point defects. Since the coinage of the term “high-entropy alloy,” including the first paper to use the name, HEAs have been suspected to exhibit “sluggish diffusion” [5]. However, the general assertion of the sluggish diffusion hypothesis in the literature without extensive experimental evidence has produced some contention within the HEA community on the topic [47]. Indeed, there are both experimental results and simulations that appear to demonstrate sluggish diffusion in the form of greater migration energies in HEAs versus pure metals (when normalizing to the homologous temperature) [48], [49], however these are outweighed by the number of studies which report a lack of evidence for universal sluggish diffusion in HEAs [50]–[54]. Nevertheless, sluggish

diffusion of point defects has been suggested as a possible explanation for the enhanced irradiation resistance experimentally observed in several HEAs. The primary hypothesis supporting sluggish diffusion is that the potential energy landscape within an HEA lattice will exhibit more peaks and valleys due to the differences in mass, interatomic forces, and lattice strain caused by presence of different atomic species occupying the same crystal lattice. Such potential energy valleys, specifically, could serve as “trapping sites” for diffusing point defects which would retard the formation of extended defects (e.g., vacancy clusters and SIA clusters) and instead the concentration of both SIAs and vacancies within the material would be greater, thus producing more sites for recombination to occur and leading to a greater rate of recombination from subsequent damage cascades. In essence, the link between sluggish diffusion of point defects and enhanced irradiation tolerance draws parallels to the very-low-temperature regime of irradiation damage evolution where in the absence of long range diffusion, point-defect concentrations saturate and extended radiation-induced defects, such as voids, never form.

Broadening/overlapping defect migration energies. Perhaps more nuanced than universal sluggish diffusion of point defects, another proposed mechanism posits that the chemical complexity of HEAs and CCAs leads to distributions of migration energies for SIAs and vacancies, which may overlap enabling enhanced defect recombination (or at least mitigate the clustering of like defects into extended structures like voids and dislocations). Since experimentally there is no clear way to measure the distribution of defect migration energies, only the effective migration energy, support for this mechanism comes almost exclusively from modeling and simulation. Indeed, many atomistic simulations have shown, primarily using binary systems, that increasing chemical complexity and solute concentration leads to a broadening distribution of defect migration energies due to the variety of different local atomic configurations in disordered solid solutions [55]–[57]. Specifically, these distributions of migration energies tend to be skewed towards slowing down the diffusion of SIAs and speeding of the diffusion of vacancies [56], [57]. By reducing the discrepancy between the diffusion rates of interstitials and vacancies, the difference in concentration between these defects is also reduced, which should increase recombination rates, since the probability of recombination is maximized when the concentrations of SIAs and vacancies are equal. However, it is unclear whether such enhanced recombination is attributable to the presence of a distribution of migration energies, or merely a reduction in the average and minimum vacancy migration energies, since migration pathways with higher energy barriers are less likely to be accessed, for example by SIAs.

Sluggish diffusion of interstitial loops/clusters. The possible sluggish diffusion of interstitial dislocation loops and clusters in HEAs is the easiest of the mechanisms discussed in this work to view experimentally. Rather than attempting to observe the diffusion of individual point defects or capture phenomena which occur on the order of picoseconds, as is the case with damage cascades, dislocation loops and clusters are large enough and move slow enough to be readily resolved through transmission electron microscopy (TEM). When interstitial atoms flee from the site of the damage cascade, they migrate toward sinks such as grain boundaries and contribute to the buildup of a vacancy supersaturation in a material. If, instead of grain boundaries, these interstitial atoms clustered together into relatively immobile dislocation loops or clusters near the damage

cascade, the probability of point defect recombination would be improved. Indeed, in several of the ion irradiation studies where reduced void swelling was observed in HEAs and CCAs interstitial dislocation loops are observed throughout the irradiated region with small voids occurring deep in the material near the peak irradiation damage, as compared to less complex metals such as pure Ni where voids are found throughout the irradiated region and dislocations are only found deep inside the material in the form of dislocation networks [58], [59]. These experimental results are also in good agreement with Molecular Dynamics simulations, which predict interstitial clusters and dislocation loops diffusing easily in 1D in pure metals (e.g., Ni) as compared to more compositionally complex alloys (e.g., NiFe, NiCo) in which interstitials clusters and dislocation loops diffuse more slowly and meander in 3D space [58]. While promising, this phenomenon has only been observed in equimolar FCC solid solutions from the Co-Cr-Fe-Mn-Ni system, thus more experimental and modeling work is necessary to determine whether such processes also play a significant role in different crystal structures and chemical systems.

While each of the above proposed mechanisms has been supported by some form of modeling and simulation, it still remains unclear which mechanism plays a dominant role in determining the performance of HEAs under irradiation. Moreover, each mechanism faces similar shortcomings and limitations, namely, the lack of experimental data. From the limited number of experimental studies that have explored the irradiation response of HEAs and CCAs, the vast majority focus on equimolar CoCrFeMnNi, or its equimolar derivatives (e.g., NiFe, NiCo). Such an approach makes isolating the effects of a single element on the irradiation response of HEAs and CCAs even more challenging, let alone the effects of multiple elements interacting, and leaves the near infinite number of non-equimolar HEA and CCA composition combinations unexplored. However, exploring a broad range of compositions quickly becomes a practical challenge given the amount of time required to synthesize, prepare, irradiate, and characterize even one new alloy using traditional metallurgical techniques. Thus, beginning with equimolar alloy compositions is often seen as a logical first step, but still remains a major compromise.

Even in the absence of daunting numbers of possible alloy compositions, certifying new materials for high-temperature nuclear applications remains an inordinately time-consuming process, as evidenced by only one new material becoming code-certified in the last 30 years [60]. Typically, modeling and simulation can be employed to provide insight and narrow the work scope in such situations; however, HEAs and CCAs pose additional challenges for many of the techniques. In the case of atomistic, first-principles modeling, disordered solid solutions can be particularly computationally expensive to model in order to accurately produce the physics of a randomized assortment of atoms. Typically, in order to achieve adequate statistical certainty, larger groups of atoms and/or many configurations of atoms must be simulated as compared to pure metals or ordered structures (e.g., oxides, intermetallics) which can result in substantially higher computation time/power requirements. An alternative to atomistic modeling in many cases is to use continuum-level modeling informed by empirical databases, such as CALculation of PHAse Diagrams (CALPHAD), which can offer immense time savings. However, HEAs and CCAs occupy the center of the alloy composition space while most historical alloy data exists on the periphery, requiring large extrapolations to make predictions about the properties of these alloys. Such models will often also rely on regular- and dilute-solution approximations when calculating properties, which can lead to greater uncertainties in the results since HEAs and CCAs, by definition, occupy the region of the composition space where these assumptions are the least accurate. Thus, even modeling and simulation suffers from the lack of experimental data on HEAs

and CCAs and the speed at which it can be generated. To efficiently explore the HEA composition space and eventually develop optimized alloys for advanced nuclear applications, a critical compilation and review of HEAs already studied will assist the effort in improving this alloy design space.

3. HIGH ENTROPY ALLOYS DATABASE DEVELOPMENT

3.1 Structural Properties Data Collection

The structural property data present in the database developed as part of this work has been collected from 2004 to present, with over 1000 HEAs across 650 unique alloy compositions and varied processing methods [5], [9], [11], [26], [61]–[146] and was acquired by either tensile or compressive loading. In addition to HEAs, over 100 common conventional alloys have been included as a basis as a standard for comparison, including steels, cast irons, and alloys of aluminum, nickel, copper, titanium, and refractory metals.

In tensile testing, a sample is shaped and placed between two wedge grips, which hold the sample in position for uniaxial tension. The sample is pulled until failure, with an extensometer present to monitor the elongation of the sample, and a recording of the stress during testing to determine stress over time [129]. Together, these produce a stress strain curve (Figure 1) from which many structural properties of each alloy can be observed and calculated. Conversely, compression testing is performed by applying a compressive load to either the middle of a thin sheet to a bulk sample to test for buckling and barreling of the sample, respectively as ways to observe the local instability of an alloy under high compressive loads [130]. Microscopy, hardness testing, and density calculations are also important and are discussed here alongside the other experimentally collected information.

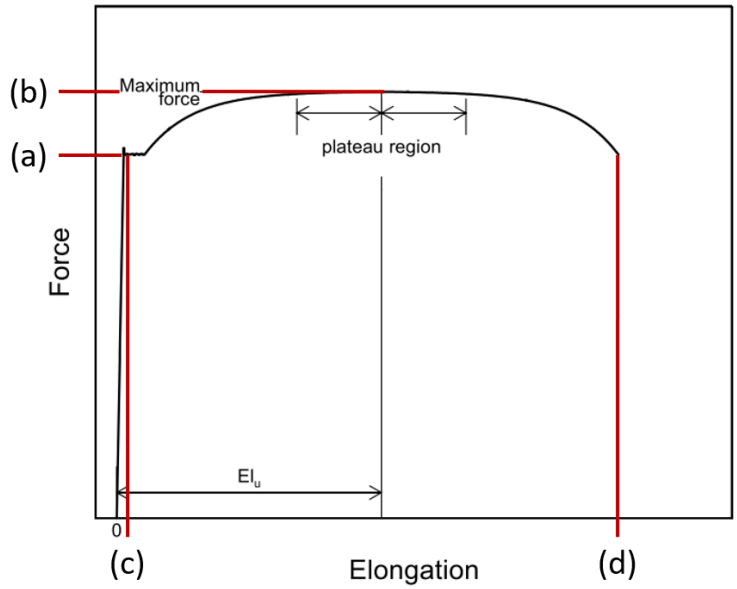

Figure 1 A plot of stress and strain typically obtained by tensile testing. The elastic modulus, (a) yield strength, (b) ultimate strength, (c) elastic elongation, and (d) plastic deformation can all be observed directly from this plot

Yield and Ultimate Strength. Yield strength is the stress level at which a material transitions from elastic (reversible) to plastic (irreversible) deformation (Figure 1a). Under standard nuclear reactor operating conditions, the ability for a material to withstand the forces imparted by pressurized water and gravity is paramount, which is why there is significant emphasis placed on yield strength during material selection. The vital nature of

this property is reflected in literature, with both over a thousand reported yield strengths for HEAs of varying composition and processing.

The maximum stress level for tensile testing before strength degradation occurs in the material is known as the ultimate strength, a property which denotes the point past which an alloy will surely fail with maintained stress (Figure 1b). This occurs past the elastic deformation zone, meaning this property is important for critical failure conditions and should not be overlooked in favor of yield strength.

Elongation. The extent to which a material will elongate under tensile stress, both elastically and plastically, is a direct measure of its ductility. Due to the relatively high loads experienced in a nuclear reactor, for instance during accidental conditions, it is assumed that the materials present could deform plastically. The elastic deformation (Figure 1c) correlates with and is just as important as the yield strength during material selection, as a low yield strength would lead to early plasticity. Plastic deformation (Figure 1d) follows the elastic regime and, much like the ultimate tensile strength, describes the maximum allowable deformation of the material prior to failure, making this valuable in reactor accident conditions.

Elastic Modulus. The elastic modulus is a measurement of stiffness for a material and is defined by the ratio of applied stress and resultant strain in the elastic regime of stress testing. The deformation response under stress, especially tensile stresses, is important, as covered by the above discussions of yield strength and elastic elongation. The elastic modulus is an additional metric with which the structural efficacy of alloys while under stress can be compared.

Density. This is a rudimentary consideration for material selection for bulk parts, and the list of environmental conditions acting upon nuclear reactor components necessitates a critical review of all impacting factors. Much like the pressure in a reactor, the force of the components imparted on one another due to their mass must be accounted for in both production and operation. In addition, neutron activation traditionally correlates with the density of alloys. For these reasons, consideration of density aids the study of HEAs.

Microstructure. The properties of metals are heavily impacted by the crystallographic structures present in the matrix. In practice, single-phase systems are preferable with a small density of secondary phases distributed intra-granularly, but this is not a guarantee with HEAs. As such, analysis of phase compositions provides insight on the impact of secondary phases on mechanical properties for prediction of alloy performance. In addition, many of the alloys present in this database have been observed with different processing and heat treatment parameters, whose impact on microstructure can be observed to determine processing procedural trends for effective single-phase HEA production.

The collected values above are not the only material property considerations, there are many properties that can be calculated from this data which provide greater insight on material characteristics and viability. Several common properties derived from tensile and compressive testing are useful for industrial implementation and have been included in this database as detailed below.

Specific Strength. While strength on its own is an asset, the strength to weight ratio is important, especially for a system as large as a nuclear reactor. The weight of the components on each other introduces additional stresses to the system, increasing the requirements for safe construction and operation. The higher the strength to weight ratio is, the less material is required for fabrication, making the comparison of specific strengths valuable in minimizing the material required for producing reactor components.

Resilience and Toughness Moduli. The resilience and toughness moduli measure the energy density within a sample when loaded to its elastic and plastic elongation limits, respectively. These are determined by measuring the area under the stress-strain curve (Figure 1) and are a function of the energy imparted on the material. While this is functionally similar to the effect of stress, additional energy sources can impact the resilience and toughness of the material. Higher resilience in a material would be indicative of greater performance under operational conditions.

This database is not limited to HEAs, however, and contains steels and refractory alloys, as well as Al-, Ni-, Cu-, and Ti-based alloys too. These provide standards for comparison between HEAs and commercially available alloys as a means of framing their relative capabilities for the properties present in this database.

3.2 Oxidation Properties Data Collection

While collecting data on the corrosion performance of HEAs is possible, data interpretation is a less straightforward task. Most corrosion experiments are tailored to their environment of interest, resulting in a wide variety of solutions and mediums for testing, ranging from common solutions like salt water to the novel molten salt environments. This variety is difficult to correlate for standard comparison across all the solutions tested, so a more modeling-focused approach of predicting oxidation performance has been chosen. In a similar fashion to alloy compositional predictions, CALPHAD modeling can provide a method of predicting the oxidation response of the alloys present in this database.

The model for predicting oxidation is based on each oxide's Gibbs free energy of formation:

$$\Delta G = \Delta G^{o} + RT ln\left(\frac{(a_{M_x O_y})^{\frac{2}{y}}}{(a_M)^{\frac{x}{y}}(a_{O_2})}\right) \tag{2}$$

$$\frac{x}{y}M + O_2 \rightarrow \frac{2}{y}M_x O_y$$

Where *a* is the chemical activity of each species in the oxidation reaction, ΔG^{o} is the standard Gibbs free energy of formation for the pure oxide. Since the result of the reaction is the pure oxide, its chemical activity can be assumed as 1, as will the environmental oxygen partial pressure since it will be held constant across all ΔG calculations. This simplifies equation 2 to the following:

$$\Delta G = \Delta G^{o} - \frac{x}{y} RT ln(a_M) \tag{3}$$

This reduces the equation to a function of the Gibb's standard energy of formation and the chemical activity of the oxide's cation in the substrate, the latter of which is approximated by

CompuTherm LLC's CALPHAD software, Pandat [147]. In this case, the chemical activities have been determined for three temperatures of interest: 500, 600, and 700 °C due to their relevance for high temperature corrosion performance. The standard energy of formation for each oxide is obtained from Metso Outotec's HSC Chemistry [148]. Thermodynamically, the oxide with the lowest Gibbs free energy of formation derived from equation 3 will be favored to form on the HEA surface first, which is the basis for corrosion performance predictions in this database.

The initial oxides forming on a surface are an indicator of its corrosion resistance, but only considering the first oxide to form does not account for many alloys which could still be protective to some degree. As such, the second most likely oxide to form, based on the predictions here, has also been included and is incorporated to further enhance the classification of predicted corrosion response.

Within the database, the five oxides predicted to form first which comprise the 90% of HEAs predicted include, in order of their relative occurrence, Al_2O_3, Cr_2O_3, MnO, TiO and VO. While alumina and chromia (Al_2O_3 and Cr_2O_3) are well documented as strong passivators and their prediction could be corroborated by literature [149]–[151], alloys with compositions comparable to those in this database which predicted MnO, TiO, and VO formation were reviewed to ensure their degree of protectiveness was well understood. While the oxides specifically predicted were not displayed, they were indicators of consistent corrosion responses. Alloys predicting either MnO or VO formation displayed mixed oxides, and neither group was protective [152]–[163]. TiO_2 formed in favor of TiO and provided corrosion resistance when paired with an alumina or chromia layer [156]–[158]. Since alumina and chromia are the driving force influencing predicted corrosion performance, the three categories of protectiveness for HEAs in this database are based on their presence and are described as follows:

Table 2. *Database oxidation resistance descriptors*

Passive	The first oxide to form is either Al_2O_3 or Cr_2O_3
Protective	Only the second oxide to form is either Al_2O_3 or Cr_2O_3
Non-Protective	Neither the first nor second oxide to form is either Al_2O_3 or Cr_2O_3

In addition to the thermodynamic prediction of surface oxidation, the diffusion of oxide cations in the substrate is also provided by Pandat calculations. While thermodynamics determine the element most likely to oxidize, the diffusion kinetics influence the rate at which cations can be supplied to the surface for sustaining the oxide formation. Since diffusion rates vary within each phase of an alloy, the rule of mixtures provides a general diffusion rate for each constituent for usage in the database. These thermodynamic and kinetic factors, together, provide insight on the nature of HEA corrosion and predict potentially corrosion resistant alloys to explore.

3.3 Ashby Plots and Property Ranking

Compilation of data is useless without a method of analysis. To better understand the data present, the database utilizes Ashby plots, devised by Michael Ashby, their namesake, for the quick comparison of the tabulated mechanical properties. The present database has been fit with an Ashby plot generator, such that any two mechanical properties available in the database may be plotted directly against each other. In addition to comparing structural properties, this database

has been constructed to allow for further refinement and down selecting of alloys based on testing parameters, method of mechanical data collection, and predicted oxidation resistance. While mechanical properties drive structural material selection, those without corrosion resistance will be quickly compromised when exposed to pressurized water conditions.

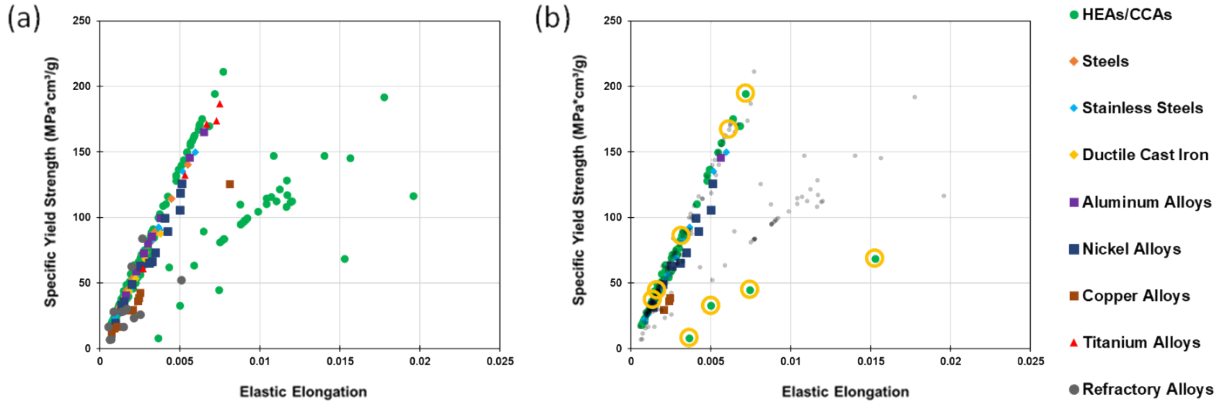

Figure 2 Ashby plots correlating elastic elongation and specific yield strength for the alloys present in this database, both as (a) the general plotted data, and (b) a plot displaying the passive oxide formers. Several Co-free HEA compositions with notable properties are circled in yellow in (b).

When considering the specific yield strength's dependence on elastic elongation (Figure 2a), one congruent positive correlation between elastic elongation and the specific yield strength is shown by commercial alloys, regardless of their basis. The HEAs tell a different story, however. While the commercial alloys present a singular trend for all alloy classes between specific yield strength and elastic elongation, the HEAs continue to present a pair of trends rather than coalescing into one like most commercial alloys (Figure 2a). Furthermore, comparing the two figures directly displays an interesting feature: while one trend is congruent with commercial alloys, the second HEA trend shows up to 2% elastic elongation at room temperature, over double that of the commercial alloys listed. Such an improvement on ductility, especially while maintaining high specific yield strength could be incredibly useful. The quick observation of trends such as this highlights the utility of this database for exploring HEAs further and informing future alloy design and selection, and this utility will expand with the database as it incorporates more material factors. In this instance, a review of the HEAs in the trend leading towards the top right corner of the above Ashby plot reveals these alloys are mostly refractory metal-based high entropy alloys (RHEAs) comprised of Hf, Nb, Ta, Ti, and Zr, while transition metal HEAs displayed a trend like that of commercial alloys. Furthermore, the heat treatment of the RHEAs in this trend suggest that it is both not optimized and has further potential to improve. These signs point to the potential benefits of tuning alloy composition and processing to improve specific strength and ductility in tandem for RHEAs.

While this is promising for structural supporting materials, exposure to corrosive environments will render these alloys ineffective as direct reactor components since refractory metals, generally, suffer from poor oxidation resistance. Considering alloys which form passive alumina and chromia oxides (Figure 2b) restricts alloys which maintain high specific yield strength, and one returns to the general trend displayed by conventional alloys in order to preserve the desired high specific yield strength. Despite this, HEAs still display improvements in both specific yield strength and elastic elongation. Many of these are variations of Cantor's alloy, CoCrCuFeNi, with substitutions

and inclusions of Al, Mo, and Ti, tout high specific yield strengths as high as 204 MPa·cm^3·g^{-1}, a 36% increase over precipitation hardened steels and over nine times greater than 316 stainless steel (21.6 MPa·cm^3·g^{-1}), which is commonly used for LWRs [60]. Cobalt, however, is a concern due to activation in LWRs, yet parsing out Co-containing alloys still provides several candidates based on the CrCuFeMnNi and AlCrFeMnNi systems with specific yield strengths on par with precipitation hardened steels and above. They continue to maintain a vast improvement in specific yield strength with over six times greater elastic elongation over 316 stainless steel as well. Like the lack of optimization in RHEAs, many of these Co-free variations of Cantor's alloy have been tested with a narrow set of processing parameters, and further exploration could lead to even greater improvements over conventional alloys in LWRs.

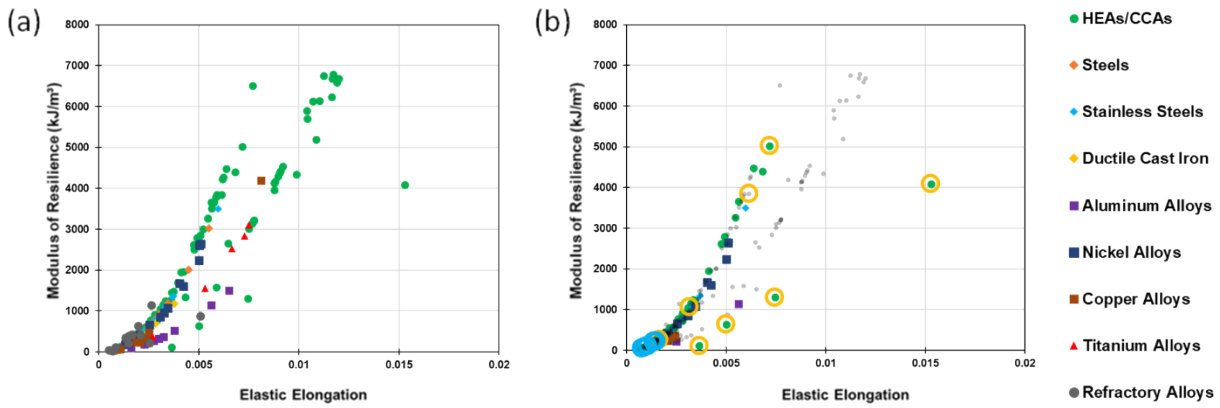

Figure 3 A plot comparing each alloy's modulus of resilience to its elastic elongation before failure for the alloys present in this database, both as (a) the general plotted data, and (b) a plot displaying the passive oxide formers. Several Co-free HEA compositions with notable properties are circled in yellow in (b).

While yield strength is a critical parameter, mechanical stresses are not the only factor for material survivability. High temperatures and other sources of energy can influence components, which is why the modulus of resilience, an energy-based measure of stiffness, is another useful consideration during material selection. In this instance, it has been compared to the elastic elongation to provide a more comprehensive look at the material performance during operation. A general trend is observed across all alloy classes that materials with greater elastic elongation also display increased resilience moduli (Figure 3a), based on the definition of the resilience modulus. Therefore, interest lies in increasing the resilience – absorbing more energy before plastically deforming – without changing elastic elongation. This corresponds to a stiffer material, one that can tolerate more aggressive operational conditions in LWRs.

HEAs begin to display greater resilience with increased elastic elongation over conventional alloys, an effect more pronounced with greater elongation (Figure 3a). Those with especially high resilience moduli are RHEAs, with some key exceptions from Cantor alloy-based HEAs. Down selecting to passivating alloys (Figure 3b), many of these improve upon both ductility and stiffness over conventional alloys. Many of these protective HEAs are Co-containing, but compositions such as AlCrCuFeNi and CrFeNiTi perform at 1000 kJ/m^3, well above ASME code certified materials like 316 stainless steel (110 kJ/m^3) and Hastelloy N (200 kJ/m^3) [60], yet these HEAs display elasticity less than half that of these conventional alloys. The brittle nature of those compositions is concerning, but there are other alternatives. AlCrFeMnNi alloys reach over 40% more energy absorbance than the top performing precipitation hardened stainless steels and

nickel alloys in the database (5020, 3500, and 2640 kJ/m^3, respectively), while still maintaining high ductility (up to 1.5% elastic elongation), exceeding both the resilience and ductility of code-certified conventional alloys. Improvements in resilience while maintaining high ductility is promising, and further highlights the potential of Co-free variations of Cantor's alloy for the nuclear industry.

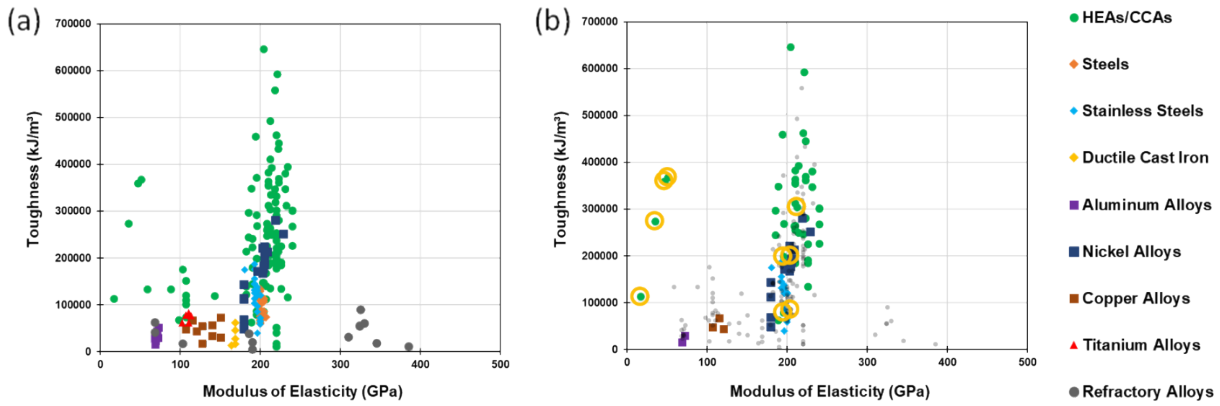

Figure 4 A comparison of the elastic and toughness moduli for the alloys present in this database, both as (a) the general plotted data, and (b) a plot displaying the passive oxide formers. Several Co-free HEA compositions with notable properties are circled in yellow in (b).

Specifically comparing the elastic modulus with an alloy's toughness is useful for failure conditions (Figure 4) and provides a more detailed look at failure than the previous Ashby plots. While Mo and W-based refractory alloys show the highest modulus of elasticity, they also display low toughness, meaning they will be highly susceptible to embrittlement and cracking. Comparing this to steels and nickel-based alloys in the figure above, it is clear why, despite their lower elastic limit, both stainless steels and nickel-based superalloys are a staple in high-stress applications. Ideally, increasing both moduli would be preferred, but current HEAs still show a marked improvement in toughness while maintaining a comparable average elastic modulus to both stainless steel and nickel-based alloys (Figure 4). Refining this Ashby plot to consider only oxidation resistant HEAs (Figure 4b), and again focusing on only Co-free alloys, CrFeNi-based HEAs with additions of Al, Cu, and Ti maintain elastic moduli near 200 GPa, on par with Ni-based alloys and stainless steels. While their elastic moduli may be comparable, their toughness is not, as these CrFeNi(Al,Cu,Ti) HEAs have reported toughness as great as 360 MJ/m^3, a vast improvement over traditional Ni alloys like Inconel 718-S, which only reach 220 MJ/m^3, which is the highest of any traditional alloy in this database. While toughness will decrease over time under reactor conditions, an increased initial toughness usually correlates to a maintained higher toughness during operation over alloys with lower initial toughness, making the higher toughness displayed by these HEAs an area of interest for accident conditions and for resisting radiation induced embrittlement (i.e. lower loss of toughness in the Ductile to Brittle Transition Temperature after irradiation). This is yet another plot which highlights the benefits of exploring Co-free Cantor alloys.

This plot can also be observed from the opposite approach – finding alloys with comparable toughness, yet a lower elastic modulus also has its benefits. In operation, a lower elastic modulus affords more ductility in the material, a useful property for forming components and avoiding total rupture of components. Several HEAs on this plot fit this ideal, with toughness on par with code-

certified materials and increased ductility as displayed by their lower elastic moduli. Figure 4 illustrates the current trend of HEAs, where producing tougher materials has been successful, yet very few HEAs maintain toughness with enhanced ductility. In particular, the AlCuCrFeNi system has several examples of this on the plot (Figure 4b), with elastic moduli as low as 35 GPa while maintaining a toughness of 274 MJ/m^3, on par with Hastelloy N (280 MJ/m^3), the toughest of the nuclear code-certified materials. This ductility difference is noteworthy – AlCuCrFeNi compositions display up to 1.53% elastic elongation, ten times that of Hastelloy N (0.14%). Not only does the plot of toughness against elastic moduli display the greater resistance to failure in accident conditions but it provides insight on ductile alloys for operational considerations without sacrificing the toughness of conventional alloys.

As a means of quickly viewing the highest performers in any category, a readout of the top performing alloys in the selected category are presented with their full dataset. This can be filtered by alloy classes to specifically look at relative performance between as few as two and as many as all nine alloy classes present in the database. To quickly compare alloy performance in all nine categories, a readout of the top performers from each alloy class is also provided in the database, such that each class can be quickly looked at together. The combination of this readout and the Ashby plots produced by the database makes for quick identification of alloys of interest and highlights the capability of Co-free variations of Cantor's alloy, particularly those containing Al, Mn, and/or Cu to surpass current materials utilized in nuclear reactors mechanically. The $Al_{(5,10)}Cr_{12}Fe_{35}Mn_{(28,23)}Ni_{20}$ and $Al_{0.3}Cu_{0.5}CrFeNi_2$ compositions are of great interest for their increased mechanical properties and potential microstructural benefits.

3.5 Alloy Compositions of Interest

While this database contains 1550 HEAs, accounting for the properties critical for nuclear implementation and data collection methods directly comparable to conventional alloys limit the total available HEAs to consider in this work, reducing the dataset of 1550 HEAs to only 65 across 19 different chemical compositions. This dataset, despite highlighting the limited list of candidate alloys, still contains several which have an advantageous blend of properties. The aforementioned $Al_{(5,10)}Cr_{12}Fe_{35}Mn_{(28,23)}Ni_{20}$ and $Al_{0.3}Cu_{0.5}CrFeNi_2$ systems both display improvements over code-certified materials mechanically, and the processing of $Al_{0.3}Cu_{0.5}CrFeNi_2$ leads to the evolution of a precipitation-hardened microstructure which may enhance radiation resistance [159], [160].

The first set of compositions, $Al_{(5,10)}Cr_{12}Fe_{35}Mn_{(28,23)}Ni_{20}$, is a set of FCC alloys which displayed comparable mechanical properties to the currently code-certified materials in their as-cast conditions. The microstructure for these compositions displayed a fully FCC crystal structure, yet optical microscopy and energy dispersive x-ray spectroscopy displayed a segregated interdentritic region rich in Al, Mn, and Ni [159]. While comparable properties are a beneficial starting point, post-processing is where these alloys shine. Both compositions were cold rolled to a 90% reduction in thickness at room temperature, and no subsequent heat treatments were performed. The resulting microstructure displayed greater chemical homogeneity over the as-cast specimens, and Elkatatny et al. found reduced deformation twinning in the microstructure overall. The work hardening of $Al_5Cr_{12}Fe_{35}Mn_{28}Ni_{20}$ and $Al_{10}Cr_{12}Fe_{35}Mn_{28}Ni_{20}$ in this study displays excellent results, with yield strengths of 1253 and 1400 MPa, more than tripling their as-cast strengths and far exceeding the 200-300 MPa strengths typical of code-certified materials [159]. While the overall ductility of these alloys drops from 42-48% to, at most, 6.78% for total elongation, the elastic elongation for each HEA increases to over 0.5% elongation, and their resilience moduli

skyrocket to at least 3.8 MJ/m^3, on par with Ti-6-4 (3.1 MJ/m^3), as well as 15-5 and 17-4 precipitation hardened steels (3.5 MJ/m^3). The increased elastic elongation allows these to return to their original shape when relaxed, avoiding permanent deformation of the components when stressed. As a work-hardened alloy with potential enhanced corrosion and irradiation resistance due to its chemical composition, the $Al_{(5,10)}Cr_{12}Fe_{35}Mn_{(28,25)}Ni_{20}$ system is a potential system of interest, even without considering further optimization.

The other main composition of interest, AlCuCrFeNi, is an alloy group which, when aged, displays high ductility, and can maintain high strength under aging conditions with the assistance of precipitate formation within the matrix. In one study, $Al_{0.3}Cu_{0.5}CrFeNi_2$ with small amounts of carbon (0.073 wt.%) displayed elastic elongation up to 1.53% coupled with a yield strength of 535 MPa, well above that of any code certified material [160]. Due to its high elasticity, its resilience moduli reached as high as 4.1 MJ/m^3 – on par with the previously discussed AlCrFeMnNi alloys, and an even greater toughness as high as 368 MJ/m^3. By comparison, the toughness of the discussed AlCrFeMnNi HEA and Hastelloy N, the toughest of the code-certified materials, are 200 and 280 MJ/m^3, respectively. The elastic deformation isn't the only property heightened in this instance, the ductility is maintained for this alloy, ranging from 39 – 98% elongation before failure. This is, at worst, slightly below the 40 – 50% total elongation code-certified materials display, but with the potential to double the ductility offered by stainless steels, even in the precipitation hardened versions of $Al_{0.3}Cu_{0.5}CrFeNi_2$. This Cu-containing alloy maintained such strength and ductility through one of its heat treatments in the work of Zhang et al; after rolling to a 20% reduction in thickness, four different conditions ranging from an annealing treatment to aging were performed [160]. With increased aging time, extremely fine precipitates formed within the matrix, both as the $L1_2$ phase and carbides, with the $L1_2$ phase forming at lower temperatures (Table 3). These precipitates are of great interest, since their size and density are on the same order of magnitude as the oxides found in oxide-dispersion strengthened (ODS) steels. ODS steels have displayed enhanced irradiation resistance that is largely attributed to their nano-scale oxide formations [161], [162]. Based on this, the nano-precipitates may also be of benefit in these alloys. Further adding to the precipitates' intrigue, they appear during the aging process, particularly in the 550 – 900 °C range, an ideal temperature range for advanced reactor systems. While the excellent mechanical properties of the AlCuCrFeNi system led to further discussion, the microstructure also displays promising potential for a mechanically sound and irradiation tolerant material.

Table 3. *The heat treatments of the C-containing $Al_{0.3}Cu_{0.5}CrFeNi_2$ system and their associated precipitation behavior*

Heat Treatment	Treatment Temperature (°C)	Treatment Time (hours)	$L1_2$ Precipitate Size (nm)	$M_{23}C_6$ Precipitate Size (nm)
A1200	1200	0.5	N/A	N/A
A550	550	150	<10 (Matrix)	50 (Grain Boundary)
A700	700	50	30 (Matrix)	30 (Acicular)
A900	900	20	Disordered $L1_2$ phase	>100 (Grain Boundary)

3.6 Database Limitations

While the data collected is useful, there are limits to its utility. Notably, the list of alloys examined is determined by the interest of researchers and industry, meaning the compositional spaces explored fall predominantly into two categories: variations of Cantor's equimolar FeCrMnNiCo alloy, and RHEAs. While this greatly expands the current compositional space, there is still a vast field of alloys which may be of interest in the future yet remain unexplored.

Composition is not the only constraint of the available data, very little mechanical testing within the temperature range of advanced reactor systems is available. As such, HEA thermal stability data is limited, and their effectiveness at operational conditions cannot be confirmed. Furthermore, this shortcoming also limits any conclusions on the creep performance of HEAs, especially due to a lack of fatigue data published. The relative infancy of HEAs as an alloy class limits the depth of testing on any given composition, and while data exists for elevated temperatures and creep testing, it is limited and cannot be effectively implemented in this database. Due to their vast compositional departure from conventional alloys, speculating on creep properties based on the available mechanical properties provides very little benefit, due to the lack of experimental data to base predictive trends off of, especially when the processing of a composition can lead to varied performance, as displayed by the works of Elkatatny et al. and Zhang et al [159], [160].

When considering the strength and toughness of the alloys in this database, the method of data collection must be acknowledged. Most research compiled here is based on either tensile or compressive testing, with very few studying their material's behavior under both conditions. While both provide valuable insight on a material's structural capabilities, compressive and tensile strength are not identical for most materials (Figure 5) yet both should be considered for accurate comparison between materials. While relying on only tensile testing would appear a simple solution since compressive failures are typically less of a concern, there are many alloys which only have compression testing data (due to the difficulty in manufacturing tensile bars), meaning they are incomparable to the tensile data present and would not be viable for analysis as structural materials in nuclear applications.

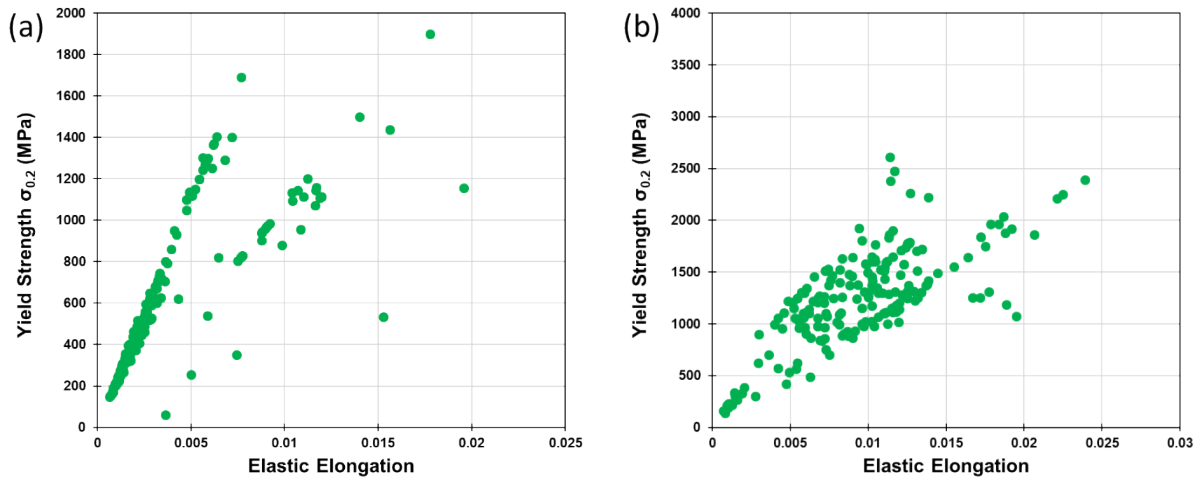

Figure 5 The yield strength data for HEAs obtained from (a) tensile and (b) compressive testing. Note the significantly higher yield strengths found when testing in compression, as well as the larger field of compressive yield strengths in comparison to the trend presented during tensile testing.

The ability to predict oxidation response in this database is also just that: a prediction, driven largely by the calculation of Gibbs free energy of formation. This results in oxide predictions such as the previously mentioned MnO, TiO, and VO, which will not form in practice and underscores the inaccuracy caused by the lack of mixed oxide characterization and knowledge. Due to the complex nature of studying mixed oxides, very little data is available that would allow for their calculation and integration into this database, and thus limits the accuracy of oxide prediction, despite still seeing success in predicting protectiveness of the surface. Additionally, while useful information is obtained through CALPHAD, diffusion data and modeling must be contextualized. The influence of kinetics is too complicated of a matter to solve with mere diffusion coefficients, it must consider factors such as oxide thickness, defect structure, growth mode, breakaway corrosion, grain boundary density, epitaxial relationship, stress state, and the influence of precipitate formation on transport. While useful for predicting potential alloys of corrosion resistant promise, the methods employed here are a means to speculate and narrow the design space for HEAs.

Another shortcoming of this database is its current inability to rank alloys based on multiparameter optimization. While a method of compositely ranking alloys based on the two properties is included in the current database alongside Ashby plots, optimizing based on multiple parameters for an all-encompassing ranking is a more nuanced issue. Its implementation requires a thorough understanding of the permissible ranges of interest for each property, as well as methods of weighting their importance over one another for a comprehensive ranking system. General methods are ineffective for the highly specific needs of many components within nuclear reactors, and HEAs are highly tunable for enhanced performance in desired areas, but not all properties at once. As such, a comprehensive ranking system is absent from this database.

4. CONCLUSIONS

The work presented herein details the production of a database cataloguing high entropy alloy mechanical testing results and calculated properties. Access to the database can be requested from Adrien Couet (couet@wisc.edu). This is supplemented with CALPHAD-based predictions of oxidation performance corroborated by literature review. This was chosen over compilation of experimental oxidation data due to lack of standardization in testing and data collection. The resultant database can generate Ashby plots for quick analysis of HEA trends in comparison to commercially available alloys. With the ability to filter by predicted oxidation response, mechanical testing methods and parameters, and provide a readout of top performers in any given categories, this database highlights the promising nature of HEAs for nuclear reactor applications and suggests that AlCuCrFeNi and AlCrFeMnNi HEAs are compositional areas of interest for future studies, and their properties have been summarized in Table 4.

While both AlCuCrFeNi and AlCrFeMnNi display enhanced operational properties over code certified materials, particularly regarding yield strength and elastic deformation, both excel elsewhere by very different means. The AlCuCrFeNi system notably provides enhanced elastic elongation alongside increased yield strength and toughness, with the added potential irradiation resistance resultant of nano-precipitates dispersed within its microstructure. Conversely, the AlCrFeMnNi alloy system shows great promise for the development of work-hardenable alloys with enhanced mechanical properties and corrosion resistance, all critical considerations for reactor materials. Despite a reduced dataset due to the constraints necessary for implementation, HEAs already display desirable properties. With further exploration and refinement of the design space, high entropy alloys will be an asset for advanced reactors and the nuclear industry as it continues to grow.

Table 4. *The mechanical properties of the $Al_{0.3}Cu_{0.5}CrFeNi_2$ and $Al_{(5,10)}Cr_{12}Fe_{35}Mn_{(28,23)}Ni_{20}$ high entropy alloys with code-certified materials for comparison*

	Yield Strength, σ = 0.2% offset		Ultimate Strength		Elongation (%)				
Alloy	(MPa)	Specific (MPa*cm³/g)	(MPa)	Specific (MPa*cm³/g)	Elastic	Total	Elastic Modulus (GPa)	Modulus of Resilience (kJ/m³)	Toughness (MJ/m³)
$Al_{0.3}Cu_{0.5}CrFeNi_2$									
A1200	62	7.95	169	21.7	0.36%	98.00%	17	113	113
A550	350	44.9	642	82.3	0.74%	73.00%	47	1303	360
A700	535	68.6	904	115.9	1.53%	39.00%	35	4089	274
A900	255	32.7	584	74.9	0.50%	88.00%	51	638	368
$Al_5Cr_{12}Fe_{35}Mn_{28}Ni_{20}$									
As Cast	280	37.3	556	74.1	0.14%	48.00%	204	192	200
Cold Rolled	1253	167.1	1392	185.6	0.61%	6.78%	204	3848	85.4
$Al_{10}Cr_{12}Fe_{35}Mn_{23}Ni_{20}$									
As Cast	320	44.4	625	86.8	0.16%	42.20%	195	263	199
Cold Rolled	1400	194.4	1500	208.3	0.72%	5.83%	195	5026	79.2
Code Certified Materials [60]									
AISI 304	207	25.9	517	64.6	0.11%	40.00%	193	111	145
AISI 316	207	25.9	517	64.6	0.11%	40.00%	193	111	145
Hastelloy N	314	35.4	794	89.6	0.14%	50.70%	219	225	280
Incoloy 800H	150	18.9	536	67.5	0.08%	50.00%	197	57.3	171
Haynes 230	310	34.6	760	84.7	0.15%	40.00%	209	230	213
Haynes 242	310	34.6	950	105.9	0.14%	40.00%	229	210	251

5. REFERENCES

[1] W. Steurer, “Single-phase high-entropy alloys A critical update,” *Mater Charact*, vol. 162, p. 110179, Apr. 2020, doi: 10.1016/j.matchar.2020.110179.

[2] B. Cantor, I. T. H. Chang, P. Knight, and A. J. B. Vincent, “Microstructural development in equiatomic multicomponent alloys,” *Materials Science and Engineering: A*, vol. 375–377, pp. 213–218, Jul. 2004, doi: 10.1016/j.msea.2003.10.257.

[3] L. L. Xiao, Z. Q. Zheng, S. W. Guo, P. Huang, and F. Wang, “Ultra-strong nanostructured CrMnFeCoNi high entropy alloys,” *Mater Des*, vol. 194, p. 108895, Sep. 2020, doi: 10.1016/j.matdes.2020.108895.

[4] F. Zhang *et al.*, “Polymorphism in a high-entropy alloy,” *Nat Commun*, vol. 8, no. 1, Jun. 2017, doi: 10.1038/ncomms15687.

[5] J.-W. Yeh *et al.*, “Nanostructured High-Entropy Alloys with Multiple Principal Elements: Novel Alloy Design Concepts and Outcomes,” *Adv Eng Mater*, vol. 6, no. 5, pp. 299–303, May 2004, doi: 10.1002/adem.200300567.

[6] O. N. Senkov, S. Rao, K. J. Chaput, and C. Woodward, “Compositional effect on microstructure and properties of NbTiZr-based complex concentrated alloys,” *Acta Mater*, vol. 151, pp. 201–215, Jun. 2018, doi: 10.1016/j.actamat.2018.03.065.

[7] D. B. Miracle, “Critical Assessment 14: High entropy alloys and their development as structural materials,” *Materials Science and Technology*, vol. 31, no. 10, pp. 1142–1147, Jan. 2015, doi: 10.1179/1743284714y.0000000749.

[8] T. Borkar *et al.*, “A combinatorial assessment of AlxCrCuFeNi2 (0~~x~~1.5) complex concentrated alloys: Microstructure, microhardness, and magnetic properties,” *Acta Mater*, vol. 116, pp. 63–76, Sep. 2016, doi: 10.1016/j.actamat.2016.06.025.

[9] Z. Wu, H. Bei, G. M. Pharr, and E. P. George, “Temperature dependence of the mechanical properties of equiatomic solid solution alloys with face-centered cubic crystal structures,” *Acta Mater*, vol. 81, pp. 428–441, Dec. 2014, doi: 10.1016/j.actamat.2014.08.026.

[10] S. Xia *et al.*, “Nonlinear Oxidation Behavior in Pure Ni and Ni-Containing Entropic Alloys,” *Front Mater*, vol. 5, Sep. 2018, doi: 10.3389/fmats.2018.00053.

[11] J.-W. Yeh, “Recent progress in high-entropy alloys,” *Annales de Chimie Science des Matériaux*, vol. 31, no. 6, pp. 633–648, Dec. 2006, doi: 10.3166/acsm.31.633-648.

[12] J.-W. Yeh, S.-Y. Chang, Y.-D. Hong, S.-K. Chen, and S.-J. Lin, “Anomalous decrease in X-ray diffraction intensities of CuNiAlCoCrFeSi alloy systems with multi-principal elements,” *Mater Chem Phys*, vol. 103, no. 1, pp. 41–46, May 2007, doi: 10.1016/j.matchemphys.2007.01.003.

[13] T. Löffler *et al.*, “Discovery of a Multinary Noble Metal-Free Oxygen Reduction Catalyst,” *Adv Energy Mater*, vol. 8, no. 34, p. 1802269, Oct. 2018, doi: 10.1002/aenm.201802269.

[14] C. Lu *et al.*, “Radiation-induced segregation on defect clusters in single-phase concentrated solid-solution alloys,” *Acta Mater*, vol. 127, pp. 98–107, Apr. 2017, doi: 10.1016/j.actamat.2017.01.019.

[15] D. B. Miracle and O. N. Senkov, “A critical review of high entropy alloys and related concepts,” *Acta Mater*, vol. 122, pp. 448–511, Jan. 2017, doi: 10.1016/j.actamat.2016.08.081.

[16] “Grain boundary segregation and intergranular fracture in molybdenum,” *Proceedings of the Royal Society of London. A. Mathematical and Physical Sciences*, vol. 370, no. 1743, pp. 431–458, Apr. 1980, doi: 10.1098/RSPA.1980.0043.

[17] A. v. Krajnikov, A. S. Drachinskiy, and V. N. Slyunyaev, “Grain boundary segregation in recrystallized molybdenum alloys and its effect on brittle intergranular fracture,” *Int J Refract Metals Hard Mater*, vol. 11, no. 3, pp. 175–180, Jan. 1992, doi: 10.1016/0263-4368(92)90060-F.

[18] J. Han, Y. Wu, J. Meng, A. Zhang, and B. Su, “Preparation of MoNbTaW Refractory High-Entropy Alloys by Spark Plasma Sintering,” *Xiyou Jinshu Cailiao Yu Gongcheng/Rare Metal Materials and Engineering*, vol. 48, no. 6, 2019.

[19] A. Vafadar, F. Guzzomi, A. Rassau, and K. Hayward, “Advances in Metal Additive Manufacturing: A Review of Common Processes, Industrial Applications, and Current Challenges,” *Applied Sciences 2021, Vol. 11, Page 1213*, vol. 11, no. 3, p. 1213, Jan. 2021, doi: 10.3390/APP11031213.

[20] J. J. Beaman, D. L. Bourell, C. C. Seepersad, and D. Kovar, “Additive Manufacturing Review: Early Past to Current Practice,” *Journal of Manufacturing Science and Engineering, Transactions of the ASME*, vol. 142, no. 11, Nov. 2020, doi: 10.1115/1.4048193/1086507.

[21] A. M. Kiss *et al.*, “Laser-Induced Keyhole Defect Dynamics during Metal Additive Manufacturing,” *Adv Eng Mater*, vol. 21, no. 10, p. 1900455, Oct. 2019, doi: 10.1002/ADEM.201900455.

[22] J. v. Gordon *et al.*, “Defect structure process maps for laser powder bed fusion additive manufacturing,” *Addit Manuf*, vol. 36, p. 101552, Dec. 2020, doi: 10.1016/J.ADDMA.2020.101552.

[23] S. Pang, X. Chen, X. Shao, S. Gong, and J. Xiao, “Dynamics of vapor plume in transient keyhole during laser welding of stainless steel: Local evaporation, plume swing and gas entrapment into porosity,” *Opt Lasers Eng*, vol. 82, pp. 28–40, Jul. 2016, doi: 10.1016/J.OPTLASENG.2016.01.019.

[24] Z. Xu *et al.*, “Corrosion resistance enhancement of CoCrFeMnNi high-entropy alloy fabricated by additive manufacturing,” *Corros Sci*, vol. 177, p. 108954, Dec. 2020, doi: 10.1016/J.CORSCI.2020.108954.

[25] O. N. Senkov, G. B. Wilks, J. M. Scott, and D. B. Miracle, “Mechanical properties of Nb25Mo25Ta25W25 and V20Nb20Mo20Ta20W20 refractory high entropy alloys,” *Intermetallics (Barking)*, vol. 19, no. 5, pp. 698–706, May 2011, doi: 10.1016/j.intermet.2011.01.004.

[26] B. Gludovatz, A. Hohenwarter, D. Catoor, E. H. Chang, E. P. George, and R. O. Ritchie, “A fracture-resistant high-entropy alloy for cryogenic applications,” *Science (1979)*, vol. 345, no. 6201, pp. 1153–1158, Sep. 2014, doi: 10.1126/science.1254581.

[27] K.-C. Lo, Y.-J. Chang, H. Murakami, J.-W. Yeh, and A.-C. Yeh, “An oxidation resistant refractory high entropy alloy protected by CrTaO4-based oxide,” *Sci Rep*, vol. 9, no. 1, May 2019, doi: 10.1038/s41598-019-43819-x.

[28] A. v Kuznetsov, D. G. Shaysultanov, N. D. Stepanov, G. A. Salishchev, and O. N. Senkov, “Tensile properties of an AlCrCuNiFeCo high-entropy alloy in as-cast and wrought conditions,” *Materials Science and Engineering: A*, vol. 533, pp. 107–118, Jan. 2012, doi: 10.1016/j.msea.2011.11.045.

[29] Y. Xin *et al.*, “High-Entropy Alloys as a Platform for Catalysis: Progress, Challenges, and Opportunities,” *ACS Catal*, vol. 10, no. 19, pp. 11280–11306, Sep. 2020, doi: 10.1021/acscatal.0c03617.

[30] Y. Yuan *et al.*, “Rare-earth high-entropy alloys with giant magnetocaloric effect,” *Acta Mater*, vol. 125, pp. 481–489, Feb. 2017, doi: 10.1016/j.actamat.2016.12.021.

[31] N. A. P. K. Kumar, C. Li, K. J. Leonard, H. Bei, and S. J. Zinkle, “Microstructural stability and mechanical behavior of FeNiMnCr high entropy alloy under ion irradiation,” *Acta Mater*, vol. 113, pp. 230–244, Jul. 2016, doi: 10.1016/j.actamat.2016.05.007.

[32] M.-R. He *et al.*, “Enhanced damage resistance and novel defect structure of CrFeCoNi under in situ electron irradiation,” *Scr Mater*, vol. 125, pp. 5–9, Dec. 2016, doi: 10.1016/j.scriptamat.2016.07.023.

[33] S. Q. Xia, X. Yang, T. F. Yang, S. Liu, and Y. Zhang, “Irradiation Resistance in Al x CoCrFeNi High Entropy Alloys,” *JOM*, vol. 67, no. 10, pp. 2340–2344, Aug. 2015, doi: 10.1007/s11837-015-1568-4.

[34] K. Jin *et al.*, “Effects of compositional complexity on the ion-irradiation induced swelling and hardening in Ni-containing equiatomic alloys,” *Scr Mater*, vol. 119, pp. 65–70, Jul. 2016, doi: 10.1016/j.scriptamat.2016.03.030.

[35] S. Xia, M. C. Gao, T. Yang, P. K. Liaw, and Y. Zhang, “Phase stability and microstructures of high entropy alloys ion irradiated to high doses,” *Journal of Nuclear Materials*, vol. 480, pp. 100–108, Nov. 2016, doi: 10.1016/j.jnucmat.2016.08.017.

[36] Y. Tong *et al.*, “Evolution of local lattice distortion under irradiation in medium- and high-entropy alloys,” *Materialia (Oxf)*, vol. 2, pp. 73–81, Oct. 2018, doi: 10.1016/j.mtla.2018.06.008.

[37] O. El-Atwani *et al.*, “Outstanding radiation resistance of tungsten-based high-entropy alloys,” *Sci Adv*, vol. 5, no. 3, Mar. 2019, doi: 10.1126/sciadv.aav2002.

[38] E. Zarkadoula and R. E. Stoller, *Primary Radiation Damage Formation in Solids*. United States: Elsevier, New York,New York,United States of America, 2020. [Online]. Available: https://www.osti.gov/biblio/1616821

[39] W. Schilling, “Properties of Frenkel defects,” *Journal of Nuclear Materials*, vol. 216, pp. 45–48, 1994, doi: https://doi.org/10.1016/0022-3115(94)90005-1.

[40] P. K. Liaw, T. Egami, C. Zhang, F. Zhang, and Y. Zhang, “Radiation behavior of high-entropy alloys for advanced reactors. Final report,” Office of Scientific and Technical Information (OSTI), Apr. 2015. doi: 10.2172/1214790.

[41] E. M. Criss and A. M. Hofmeister, “Isolating lattice from electronic contributions in thermal transport measurements of metals and alloys above ambient temperature and an adiabatic model,” *Int J Mod Phys B*, vol. 31, no. 14, p. 1750205, May 2017, doi: 10.1142/s0217979217502058.

[42] A. M. Stoneham, “Energy transfer between electrons and ions in collision cascades in solids,” *Nucl Instrum Methods Phys Res B*, vol. 48, no. 1–4, pp. 389–398, Mar. 1990, doi: 10.1016/0168-583x(90)90147-m.

[43] F. Körmann, Y. Ikeda, B. Grabowski, and M. H. F. Sluiter, “Phonon broadening in high entropy alloys,” *NPJ Comput Mater*, vol. 3, no. 1, Sep. 2017, doi: 10.1038/s41524-017-0037-8.

[44] M. Caro, L. K. Béland, G. D. Samolyuk, R. E. Stoller, and A. Caro, “Lattice thermal conductivity of multi-component alloys,” *J Alloys Compd*, vol. 648, pp. 408–413, Nov. 2015, doi: 10.1016/j.jallcom.2015.06.035.

[45] L. K. Béland *et al.*, “Features of primary damage by high energy displacement cascades in concentrated Ni-based alloys,” *J Appl Phys*, vol. 119, no. 8, p. 85901, Feb. 2016, doi: 10.1063/1.4942533.

[46] O. R. Deluigi, R. C. Pasianot, F. J. Valencia, A. Caro, D. Farkas, and E. M. Bringa, “Simulations of primary damage in a High Entropy Alloy: Probing enhanced radiation resistance,” *Acta Mater*, vol. 213, p. 116951, Jul. 2021, doi: 10.1016/j.actamat.2021.116951.

[47] S. v Divinski, A. v Pokoev, N. Esakkiraja, and A. Paul, “A Mystery of ‘Sluggish Diffusion’ in High-Entropy Alloys: The Truth or a Myth?,” *Diffusion Foundations*, vol. 17, pp. 69–104, Jul. 2018, doi: 10.4028/www.scientific.net/df.17.69.

[48] K.-Y. Tsai, M.-H. Tsai, and J.-W. Yeh, “Sluggish diffusion in CoCrFeMnNi high-entropy alloys,” *Acta Mater*, vol. 61, no. 13, pp. 4887–4897, Aug. 2013, doi: 10.1016/j.actamat.2013.04.058.

[49] J. Dabrowa, W. Kucza, G. Cieślak, T. Kulik, M. Danielewski, and J.-W. Yeh, “Interdiffusion in the FCC-structured Al-Co-Cr-Fe-Ni high entropy alloys: Experimental studies and numerical simulations,” *J Alloys Compd*, vol. 674, pp. 455–462, Jul. 2016, doi: 10.1016/j.jallcom.2016.03.046.

[50] M. Vaidya, S. Trubel, B. S. Murty, G. Wilde, and S. v Divinski, “Ni tracer diffusion in CoCrFeNi and CoCrFeMnNi high entropy alloys,” *J Alloys Compd*, vol. 688, pp. 994–1001, Dec. 2016, doi: 10.1016/j.jallcom.2016.07.239.

[51] M. Vaidya, K. G. Pradeep, B. S. Murty, G. Wilde, and S. v Divinski, “Radioactive isotopes reveal a non sluggish kinetics of grain boundary diffusion in high entropy alloys,” *Sci Rep*, vol. 7, no. 1, Sep. 2017, doi: 10.1038/s41598-017-12551-9.

[52] W. Kucza, J. Dabrowa, G. Cieślak, K. Berent, T. Kulik, and M. Danielewski, “Studies of sluggish diffusion effect in Co-Cr-Fe-Mn-Ni, Co-Cr-Fe-Ni and Co-Fe-Mn-Ni high entropy alloys determination of tracer diffusivities by combinatorial approach,” *J Alloys Compd*, vol. 731, pp. 920–928, Jan. 2018, doi: 10.1016/j.jallcom.2017.10.108.

[53] Q. Li, W. Chen, J. Zhong, L. Zhang, Q. Chen, and Z.-K. Liu, “On Sluggish Diffusion in Fcc AlCoCrFeNi High-Entropy Alloys: An Experimental and Numerical Study,” *Metals (Basel)*, vol. 8, no. 1, p. 16, Dec. 2017, doi: 10.3390/met8010016.

[54] K. Jin, C. Zhang, F. Zhang, and H. Bei, “Influence of compositional complexity on interdiffusion in Ni-containing concentrated solid-solution alloys,” *Mater Res Lett*, vol. 6, no. 5, pp. 293–299, Mar. 2018, doi: 10.1080/21663831.2018.1446466.

[55] S. Zhao, G. M. Stocks, and Y. Zhang, “Defect energetics of concentrated solid-solution alloys from ab initio calculations: Ni0.5Co0.5, Ni0.5Fe0.5, Ni0.8Fe0.2 and Ni0.8Cr0.2,” *Physical Chemistry Chemical Physics*, vol. 18, no. 34, pp. 24043–24056, 2016, doi: 10.1039/c6cp05161h.

[56] S. Zhao, “Defect properties in a VTaCrW equiatomic high entropy alloy (HEA) with the body centered cubic (bcc) structure,” *J Mater Sci Technol*, vol. 44, pp. 133–139, May 2020, doi: 10.1016/j.jmst.2019.10.025.

[57] S. Zhao, T. Egami, G. M. Stocks, and Y. Zhang, “Effect of d electrons on defect properties in equiatomic NiCoCr and NiCoFeCr concentrated solid solution alloys,” *Phys Rev Mater*, vol. 2, no. 1, Jan. 2018, doi: 10.1103/physrevmaterials.2.013602.

[58] C. Lu *et al.*, “Enhancing radiation tolerance by controlling defect mobility and migration pathways in multicomponent single-phase alloys,” *Nat Commun*, vol. 7, no. 1, Dec. 2016, doi: 10.1038/ncomms13564.

[59] T. Yang *et al.*, “The effect of injected interstitials on void formation in self-ion irradiated nickel containing concentrated solid solution alloys,” *Journal of Nuclear Materials*, vol. 488, pp. 328–337, May 2017, doi: 10.1016/j.jnucmat.2017.02.026.

[60] R. N. Wright, “Updated Draft ASME Boiler and Pressure Vessel Code Case for Use of Alloy 617 for Construction of Nuclear Components for Section III Division 5,” Office of Scientific and Technical Information (OSTI), Sep. 2018. doi: 10.2172/1471711.

[61] S. Huang, H. Wu, H. Zhu, and Z. Xie, “Effect of niobium addition upon microstructure and tensile properties of CrMnFeCoNix high entropy alloys,” *Materials Science and Engineering: A*, vol. 809, p. 140959, Mar. 2021, doi: 10.1016/J.MSEA.2021.140959.

[62] P. Cheng, Y. Zhao, X. Xu, S. Wang, Y. Sun, and H. Hou, “Microstructural evolution and mechanical properties of Al0.3CoCrFeNiSix high-entropy alloys containing coherent nanometer-scaled precipitates,” *Materials Science and Engineering: A*, vol. 772, p. 138681, Jan. 2020, doi: 10.1016/J.MSEA.2019.138681.

[63] H. C. Liu and C. W. Tsai, “Effect of Ge addition on the microstructure, mechanical properties, and corrosion behavior of CoCrFeNi high-entropy alloys,” *Intermetallics (Barking)*, vol. 132, p. 107167, May 2021, doi: 10.1016/J.INTERMET.2021.107167.

[64] L. Wang *et al.*, “Lightweight Zr1.2V0.8NbTixAly high-entropy alloys with high tensile strength and ductility,” *Materials Science and Engineering: A*, vol. 814, p. 141234, May 2021, doi: 10.1016/J.MSEA.2021.141234.

[65] V. K. Soni, S. Sanyal, and S. K. Sinha, “Phase evolution and mechanical properties of novel FeCoNiCuMox high entropy alloys,” *Vacuum*, vol. 174, p. 109173, Apr. 2020, doi: 10.1016/J.VACUUM.2020.109173.

66] R. K. Nutor, Q. P. Cao, X. D. Wang, D. X. Zhang, and J. Z. Jiang, “Tunability of the mechanical properties of (Fe50Mn27Ni10Cr13)100-xMox high-entropy alloys via secondary phase control,” *J Mater Sci Technol*, vol. 73, pp. 210–217, May 2021, doi: 10.1016/J.JMST.2020.09.029.

[67] M. Wang, Z. L. Ma, Z. Q. Xu, and X. W. Cheng, “Effects of vanadium concentration on mechanical properties of VxNbMoTa refractory high-entropy alloys,” *Materials Science and Engineering: A*, vol. 808, p. 140848, Mar. 2021, doi: 10.1016/J.MSEA.2021.140848.

[68] E. S. Panina, N. Y. Yurchenko, S. v. Zherebtsov, M. A. Tikhonovsky, M. v. Mishunin, and N. D. Stepanov, “Structures and mechanical properties of Ti-Nb-Cr-V-Ni-Al refractory high entropy alloys,” *Materials Science and Engineering: A*, vol. 786, p. 139409, Jun. 2020, doi: 10.1016/J.MSEA.2020.139409.

[69] S. Wang, Y. Zhao, P. Cheng, Q. Guo, X. Xu, and H. Hou, “Study on the mechanical properties and corrosion resistance of AlxCoFeNiCr1−x high-entropy alloys,” *Mater Res Express*, vol. 6, no. 12, p. 1265e2, Jan. 2020, doi: 10.1088/2053-1591/AB3D86.

[70] B. Kang, T. Kong, H. J. Ryu, and S. H. Hong, “Superior mechanical properties and strengthening mechanisms of lightweight AlxCrNbVMo refractory high-entropy alloys (x = 0, 0.5, 1.0) fabricated by the powder metallurgy process,” *J Mater Sci Technol*, vol. 69, pp. 32–41, Apr. 2021, doi: 10.1016/J.JMST.2020.07.012.

[71] G. Zhang *et al.*, “Effect of Co on phase stability and mechanical behavior of CoxCrFeNiMnAl0.3 high entropy alloys with micro/nano hierarchical structure,” *Mater Des*, vol. 215, p. 110442, Mar. 2022, doi: 10.1016/J.MATDES.2022.110442.

[72] C. Ji, A. Ma, and J. Jiang, “Mechanical properties and corrosion behavior of novel Al-Mg-Zn-Cu-Si lightweight high entropy alloys,” *J Alloys Compd*, vol. 900, p. 163508, Apr. 2022, doi: 10.1016/J.JALLCOM.2021.163508.

[73] Y. Jung *et al.*, “Investigation of phase-transformation path in TiZrHf(VNbTa)x refractory high-entropy alloys and its effect on mechanical property,” *J Alloys Compd*, vol. 886, p. 161187, Dec. 2021, doi: 10.1016/J.JALLCOM.2021.161187.

[74] Z. Y. Ding, B. X. Cao, J. H. Luan, and Z. B. Jiao, “Synergistic effects of Al and Ti on the oxidation behaviour and mechanical properties of L12-strengthened FeCoCrNi high-entropy alloys,” *Corros Sci*, vol. 184, p. 109365, May 2021, doi: 10.1016/J.CORSCI.2021.109365.

[75] L. Wang *et al.*, “Microstructure and mechanical properties of CoCrFeNiWx high entropy alloys reinforced by μ phase particles,” *J Alloys Compd*, vol. 843, p. 155997, Nov. 2020, doi: 10.1016/J.JALLCOM.2020.155997.

[76] J. Zhang *et al.*, “Microstructure and mechanical properties of RexNbMoTaW high-entropy alloys prepared by arc melting using metal powders,” *J Alloys Compd*, vol. 827, p. 154301, Jun. 2020, doi: 10.1016/J.JALLCOM.2020.154301.

[77] S. Wu *et al.*, “Microstructure and mechanical properties of CxHf0.25NbTaW0.5 refractory high-entropy alloys at room and high temperatures,” *J Mater Sci Technol*, vol. 97, pp. 229–238, Jan. 2022, doi: 10.1016/J.JMST.2021.05.015.

[78] C. J. Tong *et al.*, “Mechanical performance of the AlxCoCrCuFeNi high-entropy alloy system with multiprincipal elements,” *Metall Mater Trans A Phys Metall Mater Sci*, vol. 36, no. 5, pp. 1263–1271, 2005, doi: 10.1007/S11661-005-0218-9.

[79] M. Jin, P. Cao, and M. P. Short, “Thermodynamic mixing energy and heterogeneous diffusion uncover the mechanisms of radiation damage reduction in single-phase Ni-Fe alloys,” *Acta Mater*, vol. 147, pp. 16–23, Apr. 2018, doi: 10.1016/J.ACTAMAT.2017.12.064.

[80] J. M. Zhu, H. M. Fu, H. F. Zhang, A. M. Wang, H. Li, and Z. Q. Hu, “Synthesis and properties of multiprincipal component AlCoCrFeNiSix alloys,” *Materials Science and Engineering: A*, vol. 527, no. 27–28, pp. 7210–7214, Oct. 2010, doi: 10.1016/J.MSEA.2010.07.049.

[81] J. M. Zhu, H. M. Fu, H. F. Zhang, A. M. Wang, H. Li, and Z. Q. Hu, “Synthesis and properties of multiprincipal component AlCoCrFeNiSix alloys,” *Materials Science and Engineering: A*, vol. 527, no. 27–28, pp. 7210–7214, Oct. 2010, doi: 10.1016/J.MSEA.2010.07.049.

[82] N. D. Stepanov *et al.*, “Effect of V content on microstructure and mechanical properties of the CoCrFeMnNiVx high entropy alloys,” *J Alloys Compd*, vol. 628, pp. 170–185, Apr. 2015, doi: 10.1016/J.JALLCOM.2014.12.157.

[83] N. D. Stepanov, N. Y. Yurchenko, D. v. Skibin, M. A. Tikhonovsky, and G. A. Salishchev, “Structure and mechanical properties of the AlCrxNbTiV (x = 0, 0.5, 1, 1.5) high entropy alloys,” *J Alloys Compd*, vol. 652, pp. 266–280, Dec. 2015, doi: 10.1016/J.JALLCOM.2015.08.224.

[84] M. R. Chen, S. J. Lin, J. W. Yeh, S. K. Chen, Y. S. Huang, and M. H. Chuang, “Effect of vanadium addition on the microstructure, hardness, and wear resistance of Al0.5CoCrCuFeNi high-entropy alloy,” *Metallurgical and Materials Transactions A*, vol. 5, no. 37, pp. 1363–1369, 2006, doi: 10.1007/S11661-006-0081-3.

[85] N. D. Stepanov, D. G. Shaysultanov, G. A. Salishchev, and M. A. Tikhonovsky, “Structure and mechanical properties of a light-weight AlNbTiV high entropy alloy,” *Mater Lett*, vol. 142, pp. 153–155, Mar. 2015, doi: 10.1016/J.MATLET.2014.11.162.

[86] O. N. Senkov and C. F. Woodward, “Microstructure and properties of a refractory NbCrMo0.5Ta0.5TiZr alloy,” *Materials Science and Engineering: A*, vol. 529, no. 1, pp. 311–320, Nov. 2011, doi: 10.1016/J.MSEA.2011.09.033.

[87] Y. Zhang, Y. Liu, Y. X. Li, X. Chen, and H. W. Zhang, “Microstructure and Mechanical Properties of a New Refractory HfNbSi0.5TiVZr High Entropy Alloy,” *Materials Science Forum*, vol. 849, pp. 76–84, 2016, doi: 10.4028/WWW.SCIENTIFIC.NET/MSF.849.76.

[88] O. N. Senkov, J. M. Scott, S. v. Senkova, D. B. Miracle, and C. F. Woodward, “Microstructure and room temperature properties of a high-entropy TaNbHfZrTi alloy,” *J Alloys Compd*, vol. 509, no. 20, pp. 6043–6048, May 2011, doi: 10.1016/J.JALLCOM.2011.02.171.

[89] Y. D. Wu *et al.*, “A refractory Hf25Nb25Ti25Zr25 high-entropy alloy with excellent structural stability and tensile properties,” *Mater Lett*, vol. 130, pp. 277–280, Sep. 2014, doi: 10.1016/J.MATLET.2014.05.134.

[90] H. W. Yao *et al.*, “NbTaV-(Ti,W) refractory high-entropy alloys: Experiments and modeling,” *Materials Science and Engineering: A*, vol. 674, pp. 203–211, Sep. 2016, doi: 10.1016/J.MSEA.2016.07.102.

[91] Y. J. Zhou, Y. Zhang, Y. L. Wang, and G. L. Chen, “Microstructure and compressive properties of multicomponent Alx(TiVCrMnFeCoNiCu)100−x high-entropy alloys,” *Materials Science and Engineering: A*, vol. 454–455, pp. 260–265, Apr. 2007, doi: 10.1016/J.MSEA.2006.11.049.

[92] H. Chen *et al.*, “Microstructure and mechanical properties at elevated temperatures of a new Al-containing refractory high-entropy alloy Nb-Mo-Cr-Ti-Al,” *J Alloys Compd*, vol. 661, pp. 206–215, Mar. 2016, doi: 10.1016/j.jallcom.2015.11.050.

[93] K. J. Laws *et al.*, “High entropy brasses and bronzes Microstructure, phase evolution and properties,” *J Alloys Compd*, vol. 650, pp. 949–961, Nov. 2015, doi: 10.1016/j.jallcom.2015.07.285.

[94] L. Jiang *et al.*, “Effect of Mo and Ni elements on microstructure evolution and mechanical properties of the CoFeNixVMoy high entropy alloys,” *J Alloys Compd*, vol. 649, pp. 585–590, Nov. 2015, doi: 10.1016/j.jallcom.2015.07.185.

[95] Y. Zhang, X. Yang, and P. K. Liaw, “Alloy Design and Properties Optimization of High-Entropy Alloys,” *JOM*, vol. 64, no. 7, pp. 830–838, Jul. 2012, doi: 10.1007/s11837-012-0366-5.

[96] Y. D. Wu *et al.*, “Phase composition and solid solution strengthening effect in TiZrNbMoV high-entropy alloys,” *Mater Des*, vol. 83, pp. 651–660, Oct. 2015, doi: 10.1016/j.matdes.2015.06.072.

[97] H. Yao, J.-W. Qiao, M. Gao, J. Hawk, S.-G. Ma, and H. Zhou, “MoNbTaV Medium-Entropy Alloy,” *Entropy*, vol. 18, no. 5, p. 189, May 2016, doi: 10.3390/e18050189.

[98] S. Sheikh *et al.*, “Alloy design for intrinsically ductile refractory high-entropy alloys,” *J Appl Phys*, vol. 120, no. 16, p. 164902, Oct. 2016, doi: 10.1063/1.4966659.

[99] O. N. Senkov, J. M. Scott, S. v Senkova, F. Meisenkothen, D. B. Miracle, and C. F. Woodward, “Microstructure and elevated temperature properties of a refractory TaNbHfZrTi alloy,” *J Mater Sci*, vol. 47, no. 9, pp. 4062–4074, Jan. 2012, doi: 10.1007/s10853-012-6260-2.

[100] Y. Zhang, Y. Liu, Y. Li, X. Chen, and H. Zhang, “Microstructure and mechanical properties of a refractory HfNbTiVSi0.5 high-entropy alloy composite,” *Mater Lett*, vol. 174, pp. 82–85, Jul. 2016, doi: 10.1016/j.matlet.2016.03.092.

[101] S. Maiti and W. Steurer, “Structural-disorder and its effect on mechanical properties in single-phase TaNbHfZr high-entropy alloy,” *Acta Mater*, vol. 106, pp. 87–97, Mar. 2016, doi: 10.1016/j.actamat.2016.01.018.

[102] N. N. Guo *et al.*, “Microstructure and mechanical properties of refractory MoNbHfZrTi high-entropy alloy,” *Mater Des*, vol. 81, pp. 87–94, Sep. 2015, doi: 10.1016/j.matdes.2015.05.019.

[103] C.-C. Juan *et al.*, “Enhanced mechanical properties of HfMoTaTiZr and HfMoNbTaTiZr refractory high-entropy alloys,” *Intermetallics (Barking)*, vol. 62, pp. 76–83, Jul. 2015, doi: 10.1016/j.intermet.2015.03.013.

[104] C.-C. Juan *et al.*, “Solution strengthening of ductile refractory HfMo x NbTaTiZr high-entropy alloys,” *Mater Lett*, vol. 175, pp. 284–287, Jul. 2016, doi: 10.1016/j.matlet.2016.03.133.

[105] N. N. Guo *et al.*, “Microstructure and mechanical properties of in-situ MC-carbide particulates-reinforced refractory high-entropy Mo0.5NbHf0.5ZrTi matrix alloy composite,” *Intermetallics (Barking)*, vol. 69, pp. 74–77, Feb. 2016, doi: 10.1016/j.intermet.2015.09.011.

[106] O. N. Senkov, S. v Senkova, D. B. Miracle, and C. Woodward, “Mechanical properties of low-density, refractory multi-principal element alloys of the CrNbTiVZr system,” *Materials Science and Engineering: A*, vol. 565, pp. 51–62, Mar. 2013, doi: 10.1016/j.msea.2012.12.018.

[107] É. Fazakas *et al.*, “Experimental and theoretical study of Ti20Zr20Hf20Nb20X20 (X=V or Cr) refractory high-entropy alloys,” *Int J Refract Metals Hard Mater*, vol. 47, pp. 131–138, Nov. 2014, doi: 10.1016/j.ijrmhm.2014.07.009.

[108] X. Yang, Y. Zhang, and P. K. Liaw, “Microstructure and Compressive Properties of NbTiVTaAlx High Entropy Alloys,” *Procedia Eng*, vol. 36, pp. 292–298, 2012, doi: 10.1016/j.proeng.2012.03.043.

[109] S. Chen, X. Yang, K. Dahmen, P. Liaw, and Y. Zhang, “Microstructures and Crackling Noise of AlxNbTiMoV High Entropy Alloys,” *Entropy*, vol. 16, no. 2, pp. 870–884, Feb. 2014, doi: 10.3390/e16020870.

[110] C.-M. Lin, C.-C. Juan, C.-H. Chang, C.-W. Tsai, and J.-W. Yeh, “Effect of Al addition on mechanical properties and microstructure of refractory AlxHfNbTaTiZr alloys,” *J Alloys Compd*, vol. 624, pp. 100–107, Mar. 2015, doi: 10.1016/j.jallcom.2014.11.064.

[111] O. N. Senkov, C. Woodward, and D. B. Miracle, “Microstructure and Properties of Aluminum-Containing Refractory High-Entropy Alloys,” *JOM*, vol. 66, no. 10, pp. 2030–2042, Jul. 2014, doi: 10.1007/s11837-014-1066-0.

[112] K. M. Youssef, A. J. Zaddach, C. Niu, D. L. Irving, and C. C. Koch, “A Novel Low-Density, High-Hardness, High-entropy Alloy with Close-packed Single-phase Nanocrystalline Structures,” *Mater Res Lett*, vol. 3, no. 2, pp. 95–99, Dec. 2014, doi: 10.1080/21663831.2014.985855.

[113] X. Yang, S. Y. Chen, J. D. Cotton, and Y. Zhang, “Phase Stability of Low-Density, Multiprincipal Component Alloys Containing Aluminum, Magnesium, and Lithium,” *JOM*, vol. 66, no. 10, pp. 2009–2020, Jul. 2014, doi: 10.1007/s11837-014-1059-z.

[114] É. Fazakas, V. Zadorozhnyy, and D. v Louzguine-Luzgin, “Effect of iron content on the structure and mechanical properties of Al25Ti25Ni25Cu25 and (AlTi)60-xNi20Cu20Fex (x=15, 20) high-entropy alloys,” *Appl Surf Sci*, vol. 358, pp. 549–555, Dec. 2015, doi: 10.1016/j.apsusc.2015.07.207.

[115] J.-H. Pi, Y. Pan, L. Zhang, and H. Zhang, “Microstructure and property of AlTiCrFeNiCu high-entropy alloy,” *J Alloys Compd*, vol. 509, no. 18, pp. 5641–5645, May 2011, doi: 10.1016/j.jallcom.2011.02.108.

[116] S. Guo, C. Ng, J. Lu, and C. T. Liu, “Effect of valence electron concentration on stability of fcc or bcc phase in high entropy alloys,” *J Appl Phys*, vol. 109, no. 10, p. 103505, May 2011, doi: 10.1063/1.3587228.

[117] P. Jinhong, P. Ye, Z. Hui, and Z. Lu, “Microstructure and properties of AlCrFeCuNix (0.6x1.4) high-entropy alloys,” *Materials Science and Engineering: A*, vol. 534, pp. 228–233, Feb. 2012, doi: 10.1016/j.msea.2011.11.063.

[118] L. Liu, J. B. Zhu, L. Li, J. C. Li, and Q. Jiang, “Microstructure and tensile properties of FeMnNiCuCoSnx high entropy alloys,” *Mater Des*, vol. 44, pp. 223–227, Feb. 2013, doi: 10.1016/j.matdes.2012.08.019.

[119] L. Liu, J. B. Zhu, C. Zhang, J. C. Li, and Q. Jiang, “Microstructure and the properties of FeCoCuNiSnx high entropy alloys,” *Materials Science and Engineering: A*, vol. 548, pp. 64–68, Jun. 2012, doi: 10.1016/j.msea.2012.03.080.

[120] Z. Hu, Y. Zhan, G. Zhang, J. She, and C. Li, “Effect of rare earth Y addition on the microstructure and mechanical properties of high entropy AlCoCrCuNiTi alloys,” *Mater Des*, vol. 31, no. 3, pp. 1599–1602, Mar. 2010, doi: 10.1016/j.matdes.2009.09.016.

[121] B. S. Li, Y. P. Wang, M. X. Ren, C. Yang, and H. Z. Fu, “Effects of Mn, Ti and V on the microstructure and properties of AlCrFeCoNiCu high entropy alloy,” *Materials Science and Engineering: A*, vol. 498, no. 1–2, pp. 482–486, Dec. 2008, doi: 10.1016/j.msea.2008.08.025.

[122] Y. X. Zhuang, W. J. Liu, Z. Y. Chen, H. D. Xue, and J. C. He, “Effect of elemental interaction on microstructure and mechanical properties of FeCoNiCuAl alloys,” *Materials Science and Engineering: A*, vol. 556, pp. 395–399, Oct. 2012, doi: 10.1016/j.msea.2012.07.003.

[123] C. P. Lee, Y. Y. Chen, C. Y. Hsu, J. W. Yeh, and H. C. Shih, “The Effect of Boron on the Corrosion Resistance of the High Entropy Alloys Al[sub 0.5]CoCrCuFeNiB[sub x],” *J Electrochem Soc*, vol. 154, no. 8, p. C424, 2007, doi: 10.1149/1.2744133.

[124] X. F. Wang, Y. Zhang, Y. Qiao, and G. L. Chen, “Novel microstructure and properties of multicomponent CoCrCuFeNiTix alloys,” *Intermetallics (Barking)*, vol. 15, no. 3, pp. 357–362, Mar. 2007, doi: 10.1016/j.intermet.2006.08.005.

[125] C.-J. Tong *et al.*, “Microstructure characterization of Al x CoCrCuFeNi high-entropy alloy system with multiprincipal elements,” *Metallurgical and Materials Transactions A*, vol. 36, no. 4, pp. 881–893, Apr. 2005, doi: 10.1007/s11661-005-0283-0.

[126] C.-M. Lin, H.-L. Tsai, and H.-Y. Bor, “Effect of aging treatment on microstructure and properties of high-entropy Cu0.5CoCrFeNi alloy,” *Intermetallics (Barking)*, vol. 18, no. 6, pp. 1244–1250, Jun. 2010, doi: 10.1016/j.intermet.2010.03.030.

[127] Y. Dong, Y. Lu, J. Kong, J. Zhang, and T. Li, “Microstructure and mechanical properties of multi-component AlCrFeNiMox high-entropy alloys,” *J Alloys Compd*, vol. 573, pp. 96–101, Oct. 2013, doi: 10.1016/j.jallcom.2013.03.253.

[128] S.-T. Chen *et al.*, “Microstructure and properties of age-hardenable AlxCrFe1.5MnNi0.5 alloys,” *Materials Science and Engineering: A*, vol. 527, no. 21–22, pp. 5818–5825, Aug. 2010, doi: 10.1016/j.msea.2010.05.052.

[129] J. Y. He *et al.*, “Effects of Al addition on structural evolution and tensile properties of the FeCoNiCrMn high-entropy alloy system,” *Acta Mater*, vol. 62, pp. 105–113, Jan. 2014, doi: 10.1016/j.actamat.2013.09.037.

[130] Y. J. Zhou, Y. Zhang, Y. L. Wang, and G. L. Chen, “Solid solution alloys of AlCoCrFeNiTix with excellent room-temperature mechanical properties,” *Appl Phys Lett*, vol. 90, no. 18, p. 181904, Apr. 2007, doi: 10.1063/1.2734517.

[131] F. J. Wang, Y. Zhang, and G. L. Chen, “Atomic packing efficiency and phase transition in a high entropy alloy,” *J Alloys Compd*, vol. 478, no. 1–2, pp. 321–324, Jun. 2009, doi: 10.1016/j.jallcom.2008.11.059.

[132] C.-C. Juan *et al.*, “On microstructure and mechanical performance of AlCoCrFeMo0.5Nix high-entropy alloys,” *Intermetallics (Barking)*, vol. 32, pp. 401–407, Jan. 2013, doi: 10.1016/j.intermet.2012.09.008.

[133] C.-Y. Hsu, W.-R. Wang, W.-Y. Tang, S.-K. Chen, and J.-W. Yeh, “Microstructure and Mechanical Properties of New AlCoxCrFeMo0.5Ni High-Entropy Alloys,” *Adv Eng Mater*, vol. 12, no. 1–2, pp. 44–49, Feb. 2010, doi: 10.1002/adem.200900171.

[134] S. G. Ma and Y. Zhang, “Effect of Nb addition on the microstructure and properties of AlCoCrFeNi high-entropy alloy,” *Materials Science and Engineering: A*, vol. 532, pp. 480–486, Jan. 2012, doi: 10.1016/j.msea.2011.10.110.

[135] J. M. Zhu, H. M. Fu, H. F. Zhang, A. M. Wang, H. Li, and Z. Q. Hu, “Microstructure and compressive properties of multiprincipal component AlCoCrFeNiCx alloys,” *J Alloys Compd*, vol. 509, no. 8, pp. 3476–3480, Feb. 2011, doi: 10.1016/j.jallcom.2010.10.047.

[136] J. M. Zhu, H. M. Fu, H. F. Zhang, A. M. Wang, H. Li, and Z. Q. Hu, “Microstructures and compressive properties of multicomponent AlCoCrFeNiMox alloys,” *Materials Science and Engineering: A*, vol. 527, no. 26, pp. 6975–6979, Oct. 2010, doi: 10.1016/j.msea.2010.07.028.

[137] Y. P. Wang, B. S. Li, M. X. Ren, C. Yang, and H. Z. Fu, “Microstructure and compressive properties of AlCrFeCoNi high entropy alloy,” *Materials Science and Engineering: A*, vol. 491, no. 1–2, pp. 154–158, Sep. 2008, doi: 10.1016/j.msea.2008.01.064.

[138] C. Li, J. C. Li, M. Zhao, and Q. Jiang, “Effect of alloying elements on microstructure and properties of multiprincipal elements high-entropy alloys,” *J Alloys Compd*, vol. 475, no. 1–2, pp. 752–757, May 2009, doi: 10.1016/j.jallcom.2008.07.124.

[139] W. Chen, Z. Fu, S. Fang, H. Xiao, and D. Zhu, “Alloying behavior, microstructure and mechanical properties in a FeNiCrCo0.3Al0.7 high entropy alloy,” *Mater Des*, vol. 51, pp. 854–860, Oct. 2013, doi: 10.1016/j.matdes.2013.04.061.

[140] B. S. Murty, J. W. Yeh, and S. Ranganathan, “High-Entropy Alloys,” in *High Entropy Alloys*, Elsevier, 2014, pp. 13–35. doi: 10.1016/b978-0-12-800251-3.00002-x.

[141] M.-H. Chuang, M.-H. Tsai, W.-R. Wang, S.-J. Lin, and J.-W. Yeh, “Microstructure and wear behavior of AlxCo1.5CrFeNi1.5Tiy high-entropy alloys,” *Acta Mater*, vol. 59, no. 16, pp. 6308–6317, Sep. 2011, doi: 10.1016/j.actamat.2011.06.041.

[142] K. B. Zhang *et al.*, “Microstructure and mechanical properties of CoCrFeNiTiAlx high-entropy alloys,” *Materials Science and Engineering: A*, vol. 508, no. 1–2, pp. 214–219, May 2009, doi: 10.1016/j.msea.2008.12.053.

[143] C.-Y. Hsu, C.-C. Juan, T.-S. Sheu, S.-K. Chen, and J.-W. Yeh, “Effect of Aluminum Content on Microstructure and Mechanical Properties of Al x CoCrFeMo0.5Ni High-Entropy Alloys,” *JOM*, vol. 65, no. 12, pp. 1840–1847, Sep. 2013, doi: 10.1007/s11837-013-0753-6.

[144] Y.-F. Kao, T.-J. Chen, S.-K. Chen, and J.-W. Yeh, “Microstructure and mechanical property of as-cast, -homogenized, and -deformed AlxCoCrFeNi (0x2) high-entropy alloys,” *J Alloys Compd*, vol. 488, no. 1, pp. 57–64, Nov. 2009, doi: 10.1016/j.jallcom.2009.08.090.

[145] W. H. Liu, J. Y. He, H. L. Huang, H. Wang, Z. P. Lu, and C. T. Liu, “Effects of Nb additions on the microstructure and mechanical property of CoCrFeNi high-entropy alloys,” *Intermetallics (Barking)*, vol. 60, pp. 1–8, May 2015, doi: 10.1016/j.intermet.2015.01.004.

[146] T. T. Zuo, R. B. Li, X. J. Ren, and Y. Zhang, “Effects of Al and Si addition on the structure and properties of CoFeNi equal atomic ratio alloy,” *J Magn Magn Mater*, vol. 371, pp. 60–68, Dec. 2014, doi: 10.1016/j.jmmm.2014.07.023.

[147] “Pandat Software: CALPHAD-based materials design – CompuTherm.” https://computherm.com/software (accessed Jun. 24, 2022).

[148] “HSC Chemistry - Metso Outotec.” https://www.mogroup.com/portfolio/hsc-chemistry/ (accessed Jun. 24, 2022).

[149] M. Garg, H. S. Grewal, R. K. Sharma, B. Gwalani, and H. S. Arora, “High oxidation resistance of AlCoCrFeNi high entropy alloy through severe shear deformation processing,” *J Alloys Compd*, vol. 917, p. 165385, Oct. 2022, doi: 10.1016/J.JALLCOM.2022.165385.

[150] H. Shimizu, M. Yuasa, H. Miyamoto, and K. Edalati, “Corrosion Behavior of Ultrafine-Grained CoCrFeMnNi High-Entropy Alloys Fabricated by High-Pressure Torsion,” *Materials 2022, Vol. 15, Page 1007*, vol. 15, no. 3, p. 1007, Jan. 2022, doi: 10.3390/MA15031007.

[151] J. Zhu *et al.*, “High-Temperature Oxidation Behaviours of AlCoCrFeNi High-Entropy Alloy at 1073–1273 K,” *Oxidation of Metals*, vol. 94, no. 3–4, pp. 265–281, Oct. 2020, doi: 10.1007/S11085-020-09991-6.

[152] N. A. Shaburova, A. O. Moghaddam, S. N. Veselkov, M. v. Sudarikov, O. v. Samoilova, and E. A. Trofimov, “High-Temperature Oxidation Behavior of AlxCoCrFeNiM (M = Cu, Ti, V) High-Entropy Alloys,” *Physical Mesomechanics*, vol. 24, no. 6, pp. 653–662, Dec. 2021, doi: 10.1134/S1029959921060035.

[153] M. Huang, C. Wang, H. Cui, W. Zhang, and C. Zhang, “Investigation of the structure and properties of AlCrCuFeNiVx high-entropy alloys,” *Vacuum*, vol. 173, p. 109129, Mar. 2020, doi: 10.1016/J.VACUUM.2019.109129.

[154] S. Pratskova, O. Samoilova, E. Ageenko, N. Shaburova, A. O. Moghaddam, and E. Trofimov, “Corrosion Resistance of AlxCoCrFeNiM (M = Ti, V, Si, Mn, Cu) High Entropy Alloys in NaCl and H2SO4 Solutions,” *Metals 2022, Vol. 12, Page 352*, vol. 12, no. 2, p. 352, Feb. 2022, doi: 10.3390/MET12020352.

[155] M. M. Ali, S. S. Abd Elmoamen, M. A. H. Gepreel, H. A. Ahmed, and F. A. Elrefaie, “High temperature oxidation of non equi-atomic Al5Cr12Fe35Mn28Ni20 high entropy alloy,” *Mater Res Express*, vol. 8, no. 3, p. 036508, Mar. 2021, doi: 10.1088/2053-1591/ABEAB9.

[156] T. M. Butler and K. J. Chaput, “Native oxidation resistance of Al20Nb30Ta10Ti30Zr10 refractory complex concentrated alloy (RCCA),” *J Alloys Compd*, vol. 787, pp. 606–617, May 2019, doi: 10.1016/J.JALLCOM.2019.02.128.

[157] B. Gorr *et al.*, “High temperature oxidation behavior of an equimolar refractory metal-based alloy 20Nb20Mo20Cr20Ti20Al with and without Si addition,” *J Alloys Compd*, vol. 688, pp. 468–477, Dec. 2016, doi: 10.1016/J.JALLCOM.2016.07.219.

[158] D. Sun *et al.*, “High-temperature oxidation and wear properties of TiC-reinforced CrMnFeCoNi high entropy alloy composite coatings produced by laser cladding,” *Surf Coat Technol*, vol. 438, p. 128407, May 2022, doi: 10.1016/J.SURFCOAT.2022.128407.

[159] S. Elkatatny, M. A. H. Gepreel, A. Hamada, K. Nakamura, K. Yamanaka, and A. Chiba, “Effect of Al content and cold rolling on the microstructure and mechanical properties of Al5Cr12Fe35Mn28Ni20 high-entropy alloy,” *Materials Science and Engineering: A*, vol. 759, pp. 380–390, 2019, doi: https://doi.org/10.1016/j.msea.2019.05.056.

[160] K. Zhang, H. Wen, B. Zhao, X. Dong, and L. Zhang, “Precipitation behavior and its impact on mechanical properties in an aged carbon-containing Al0.3Cu0.5CrFeNi2 high-entropy alloy,” *Mater Charact*, vol. 155, p. 109792, 2019, doi: https://doi.org/10.1016/j.matchar.2019.109792.

[161] V. v Sagaradze *et al.*, “Radiation resistance and thermal creep of ODS ferritic steels,” *Journal of Nuclear Materials*, vol. 295, no. 2, pp. 265–272, 2001, doi: https://doi.org/10.1016/S0022-3115(01)00511-6.

[162] A. Certain, S. Kuchibhatla, V. Shutthanandan, D. T. Hoelzer, and T. R. Allen, “Radiation stability of nanoclusters in nano-structured oxide dispersion strengthened (ODS) steels,” *Journal of Nuclear Materials*, vol. 434, no. 1, pp. 311–321, 2013, doi: https://doi.org/10.1016/j.jnucmat.2012.11.021.

TLR-RES/DE/REB-2023-01, "Use of High Entropy Alloys (HEAs) in Future Nuclear Applications" DATE January 31, 2023

DISTRIBUTION:
RFurstenau, RES
JTappert, RES/DRA
LLund, RES/DE
JMcKirgan, RES/DE
RTregoning, RES/DE
MRahimi, NMSS/DFM/MSB
JSteckel, RES/DE/RGGIB
MHayes, NRR/DANU/UTB1
CDeMessieres, NRR
DRudland, NRR/DNRL

ADAMS Accession No.: ML23030B836; ML23030B838

OFFICE	RES/DE/CMB	RES/DE/CIB		
NAME	WReed *WR*	RIyengar *RI*		
DATE	Jan 30, 2023	Jan 31, 2023		

OFFICIAL RECORD COPY